Geological Magazine

www.cambridge.org/geo

Original Article

Cite this article: Dai Y, Ma L, Wang C, Li T, and He HY. Homogeneous He-Ar-S-Pb isotopic compositions of new-type stratiform Cu deposits in the Jianglang Dome, southeastern Songpan-Ganze Orogen. *Geological Magazine* **163**(e19): 1–16. https://doi.org/10.1017/S0016756826100648

Received: 18 September 2025
Revised: 9 March 2026
Accepted: 23 March 2026

Keywords:
Epigenetic mineralization; magmatic-hydrothermal system; crustal origin; source homogeneity; stratiform Cu deposits

Corresponding authors:
Yanpei Dai; Email: diyeplas@foxmail.com;
Long Ma; Email: 85230988@qq.com

Homogeneous He-Ar-S-Pb isotopic compositions of new-type stratiform Cu deposits in the Jianglang Dome, southeastern Songpan-Ganze Orogen

Yanpei Dai[1], Long Ma[1], Changnan Wang[2], Tongzhu Li[1] and HuaiYu He[3]

[1]Chengdu Center, China Geological Survey (Geosciences Innovation Center of Southwest China), Ministry of Natural Resources, Chengdu 610218, China; [2]Sichuan Liwu Copper Company Limited, Kangding 626099, China and [3]State Key Laboratory of Lithospheric Evolution, Institute of Geology and Geophysics, Chinese Academy of Sciences, Beijing 100029, China

Abstract

New-type metasedimentary rock-hosted stratiform Cu deposits occur in the Jianglang Dome. They are hosted by the Late Neoproterozoic Liwu Group and were unusually induced by an epigenetic magmatic-hydrothermal system. However, the source characteristics of fluids and metals remain poorly understood. Here, we employed Re-Os dating and He-Ar-S-Pb isotopes to determine their mineralization age and origin. Chalcopyrite Re-Os isotopic dating defines an isochron age of 162.7 ± 3.2 Ma and a crust-like initial $^{187}Os/^{188}Os$ ratio of 1.421 ± 0.021 ($n = 4$). Sulphide He-Ar isotope ($n = 20$) yields low R/Ra ratios of 0.052–0.144, high $^{40}Ar/^{36}Ar$ ratios of 479–2463 and low $^{40}Ar^*/^4He$ ratios of 0.013–0.804, with calculated He_{mantle} values of 0.69–2.20 wt.%. In situ chalcopyrite sulphur isotope exhibits positive $\delta^{34}S_{V\text{-}CDT}$ values of 3.87–9.50‰ ($n = 72$). Together with similar lead isotope data of chalcopyrite separates ($n = 40$) and ca. 164 Ma granites ($n = 4$), as well as low residual gravity anomalies in this region, our integrated data indicate an epigenetic magmatic-hydrothermal mineralization at ca. 163 Ma. The ore-forming fluids were dominantly crust-derived, with minor air-saturated water and negligible mantle input (0.69–2.20 wt.%). This is most likely attributed to the low proportion (total <5 vol%) of sandwiched metabasic rocks in the metalliferous Liwu Group. All the investigated orebodies show source homogeneity, in contrast to classic sediment-hosted stratiform Cu deposits with isotopic heterogeneity. Further, our findings imply significant mineral exploration potential in the Jianglang Dome and analogous domes in the eastern Songpan-Ganze Orogen.

1. Introduction

Sediment-hosted stratiform Cu (SSC) deposits, with a typical high Cu grade of 1.52%, provide more than 10% of the world's copper resources (Mudd and Jowitt, 2018) and are an important source of cobalt (63%, Horn *et al.* 2021) and other metals. These deposits form when cupriferous hydrothermal fluids are transported across reduction fronts (e.g. carbonaceous shales or dolomites) and triggered copper sulphide precipitation (Hitzman *et al.* 2010; Borg *et al.* 2012; Brown, 2014). The SSC deposits are associated with oxidized, saline and acid hydrothermal fluids, such as low-to moderate-temperature basinal brines and high-temperature saline fluids (Dewaele *et al.* 2006; El Desouky *et al.* 2009; Davey *et al.* 2021; Qiu *et al.* 2021; Mambwe *et al.* 2024). In some cases, the SSC deposits are hosted by metasedimentary sequences of anchi-metamorphic to amphibolite-facies, and granitic intrusions are commonly absent (Hitzman *et al.* 2010; Brown, 2014; Hayes *et al.* 2015). This is exemplified by typical SSC deposits in the Central African Copperbelt, the Udokan district of Russia and the Zhongtiao Mountains of the North China Craton (Table 1). Previous studies have shown that magmatic exsolution of chlorine gives rise to saline fluids, which are effective for metal remobilization and transportation (Audétat and Edmonds, 2020; Virtanen *et al.* 2021). However, significant examples of SSC deposits related to magmatic-hydrothermal systems have been little documented.

In the southeastern Songpan-Ganze Orogen, a suite of high-grade (average 1.75%) stratiform Cu deposits occurs in the Jianglang Dome, which is intruded by granitic plutons (Figure 1). These deposits are hosted by a metamorphosed siliciclastic sequence of the Late Neoproterozoic Liwu Group (544.5–538.8 Ma, Dai *et al.* 2025a). They share similarities to classic SSC deposits, which were commonly ascribed to diagenetic hydrothermal and synorogenic mineralization (Table 1), and partially suffered complex tectonic superimposition and replacement (e.g. Brown, 2014; Muchez *et al.* 2015; Höhn *et al.* 2017; Qiu *et al.* 2021). More recently, according to chalcopyrite Re-Os and hydrothermal zircon U-Pb dating results, Dai *et al.* (2025b) proposed two-staged formation for stratiform Cu deposits in the Jianglang Dome, including: (1) ca. 550

Table 1. Detailed comparison of classic SSC deposits and stratiform Cu deposits in the Jianglang Dome (modified after Dai *et al.* 2025b)

Location	Central African Copperbelt	Udokan	Zhongtiao Mountains	Jianglang Dome
Ore grade	Cu@3%	Cu@0.72–1.50%	Cu@1.2%	Cu@1.75%
Ore mineral	Chalcocite, bornite, chalcopyrite, carrollite, Co-rich pyrite and pyrrhotite	Chalcocite, bornite, chalcopyrite, pyrrhotite, haematite and magnetite	Chalcopyrite, Co-rich pyrite, pyrrhotite and siegenite	Chalcopyrite and pyrrhotite
Alteration type	Silicic, dolomitic, albitic, potassic and calcic	Silicic, biotitic, sericitic and epidotic	Silicic, dolomitic, biotitic and albitic	Silicic, biotitic, sericitic and chloritic
Mineralization style	Disseminated, massive, veinlet, lenses and nodules	Disseminated, massive, veinlet, lenses and nodules	Disseminated, massive, veinlet, and lenses	Disseminated, massive, banded and lenses
Orebody shape	Stratiform and cross-cutting	Stratiform and lenticular	Stratiform and lenticular	Stratiform and lenticular
Orebody extension	Continuous	Continuous	Continuous	Continuous
Age and strata of host rock	820–727 Ma Roan Group	2180–2066 Ma Chinei Group	2089–2056 Ma Zhongtiao Group	~545 Ma Liwu Group
Lithology of host rock	Siltstone, mudstone, dolomite, dolomitic shale and evaporite	Sandstone, siltstone, silty shale and calcareous shale	Graphite schist, marble and meta-evaporite	Two-mica quartz schist, quartzite and minor metabasic rocks
Metamorphic grade	Anchimetamorphic to amphibolite	Greenschist to amphibolite	Greenschist to amphibolite	Greenschist to amphibolite
Redox boundary	Carbonaceous shale and dolomite	Black schist and sulphidized shale	Graphite schist	Carbonaceous schist
Diagenetic hydrothermal mineralization	787–645 Ma	2180–2066 Ma	2089–2056 Ma	~549 Ma
Synorogenic mineralization	548–473 Ma	1896 Ma	1952–1819 Ma	Nonexistent
Granitic intrusion	Nonexistent	Nonexistent	Nonexistent	~164 Ma post-orogenic granite
Magmatic-hydrothermal mineralization	Nonexistent	Nonexistent	Nonexistent	~163 Ma
Metal source	Fertile redbed and basement rocks	Fertile metasedimentary rocks formed in subareal environment	Fertile basement rocks formed in transgression events	Fertile basement rocks formed in a back-arc basin
Leaching fluid	Primary basinal brine and epigenetic hydrothermal fluid	Primary basinal brine and epigenetic metamorphic fluid	Primary basinal brine and epigenetic metamorphic fluid	Magmatic-hydrothermal fluid
Epigenetic fluid property	Temperature of 37–385 °C salinity of 0.71–45.5 wt.% NaCl CO_2-poor	Temperature of 192–222 °C salinity of 2.6–2.7 wt.% NaCl CO_2-rich	Temperature of 178–363 °C salinity of 7.3–37.0 wt.% NaCl CO_2-rich with minor CH_4	Temperature of 142–375 °C salinity of 5.26–21.19 wt.% NaCl CH_4-rich with minor CO_2
Sulphide $\delta^{34}S_{V\text{-}CDT}$ value	−16.0‰ to 21.0‰	−8.1‰ to 13.5‰	3.4–22.2‰	3.87–9.50‰
Main references	Selley *et al.* 2005; El Desouky *et al.* 2010; Bernau *et al.* 2013; Schmandt *et al.* 2013; Muchez *et al.* 2010, 2015; Sillitoe *et al.* 2017; Liu *et al.* 2024; Mambwe *et al.* 2024	Perelló *et al.* 2017; Gongalsky *et al.* 2024	Qiu *et al.* 2016, 2017, 2021; Zhao *et al.* 2018	Dai *et al.* 2017, 2025a, 2025b; Yuan *et al.* 2023 and this study

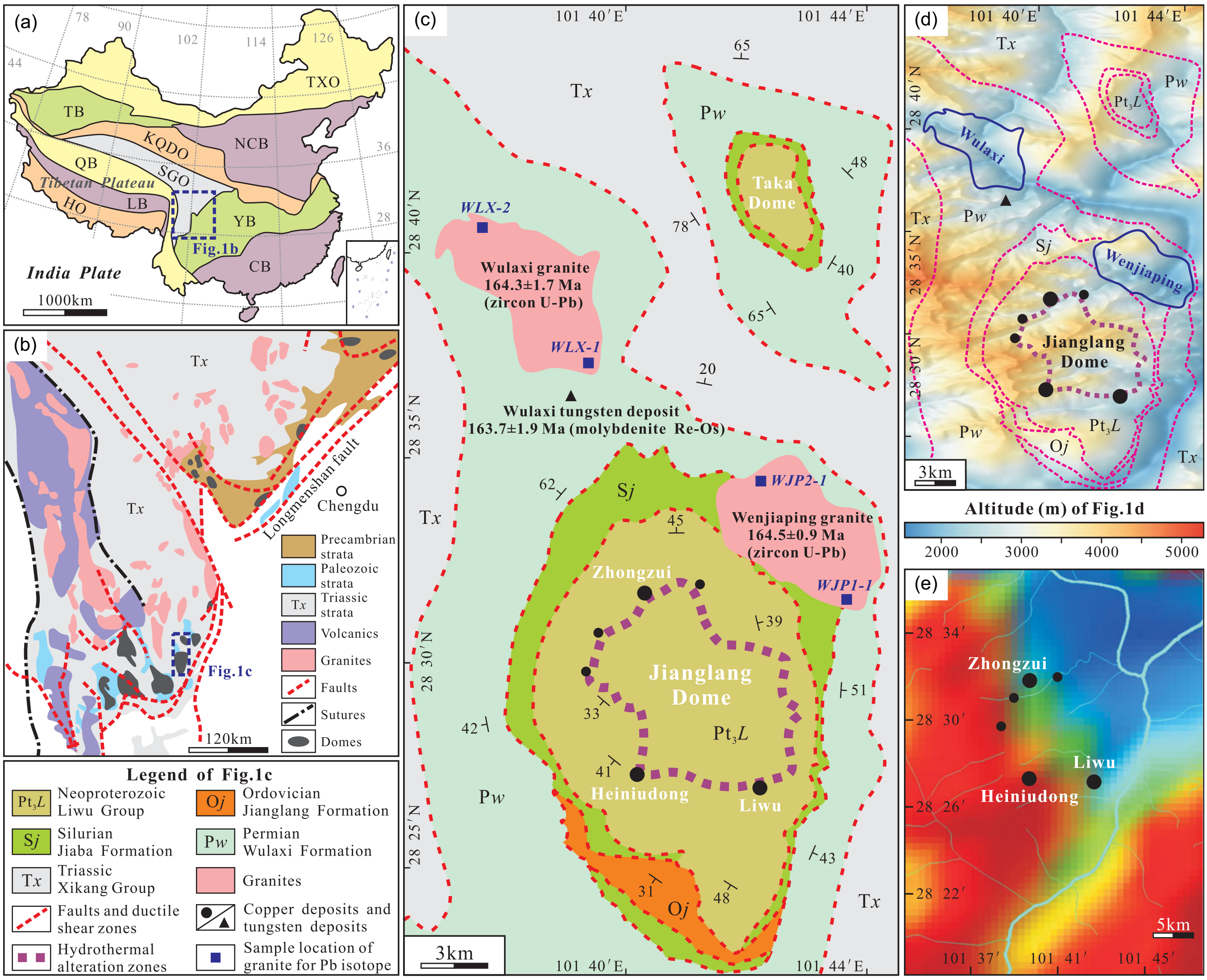

Figure 1. (a) Simplified tectonic division map of China, TXO = Tianshan-Xingmeng Orogen, TB = Tarim Block, NCB = North China Block, KQDO = Kunlun-Qinling-Dabie Orogen, SGO = Songpan-Ganze Orogen, YB = Yangtze Block, CB = Cathaysia Block. (b) Regional geological map of the eastern Tibetan Plateau. (c–d) Geological and topographical map of the Jianglang Dome. (e) The residual gravity anomaly map of the Jianglang Dome and its vicinity, note that warm colours indicate high gravity, while cool colours indicate low gravity.

Ma syngenetic enrichment; and (2) ca. 160 Ma epigenetic magmatic-hydrothermal reactivation related to ca. 164 Ma granite. This thereby indicates a superimposed genetic model and a new type of granitic intrusion-related, metasedimentary rock-hosted stratiform Cu deposit (Dai *et al.* 2025b). Nevertheless, the source characteristics of fluids and metals remain poorly understood.

In this study, we revisited typical stratiform Cu deposits in the Jianglang Dome, and we used chalcopyrite Re-Os dating and sulphide He-Ar-S-Pb isotope systematics to determine their mineralization age and origin. In conjunction with previous studies, our combined data illuminate a dominantly crustal origin for fluids and metals, as well as source homogeneity in the investigated stratiform Cu deposits.

2. Geological setting

2.a. Regional geology

The Songpan-Ganze Orogen covers a triangular-shaped area of about 2.2×10^5 km^2 in the eastern Tibetan Plateau (Figure 1a). It is the result of interactions between the Yangtze, North China and Qiangtang Blocks during the Indosinian Orogeny (Early Triassic to Early Jurassic), which were induced by the closing of the Palaeo-Tethys Ocean (Roger *et al.* 2010; Xu *et al.* 2020). The Neoproterozoic crystalline basement, probably with an oceanic crust nature, only crops out in the southern part of the Songpan-Ganze Orogen and is locally migmatized and ductilely deformed (Roger *et al.* 2010). The Songpan-Ganze Orogen is exclusively overlain by 5–15 km thick Triassic flysch deposits that received materials from adjacent blocks (Weislogel *et al.* 2010). These flysch deposits are composed of alternating shale and sandstone, with minor carbonate and greywacke. They suffered greenschist-to amphibolite-facies Barrovian metamorphism during the Late Indosinian crustal thickening and shortening (ca. 205–190 Ma, Huang *et al.* 2003a, 2003b) and were intruded by widespread granitic plutons (Figure 1b). Based on tectonic, geochemical and geochronological studies, these granitoids were divided in two groups: (1) syn-to late-orogenic at ca. 220–200 Ma; and (2) post-orogenic at ca. 200–150 Ma (Roger *et al.* 2004, 2010). The syn-orogenic granitoids were formed in a syn-collisional to

https://doi.org/10.1017/S0016756826100648 Published online by Cambridge University Press

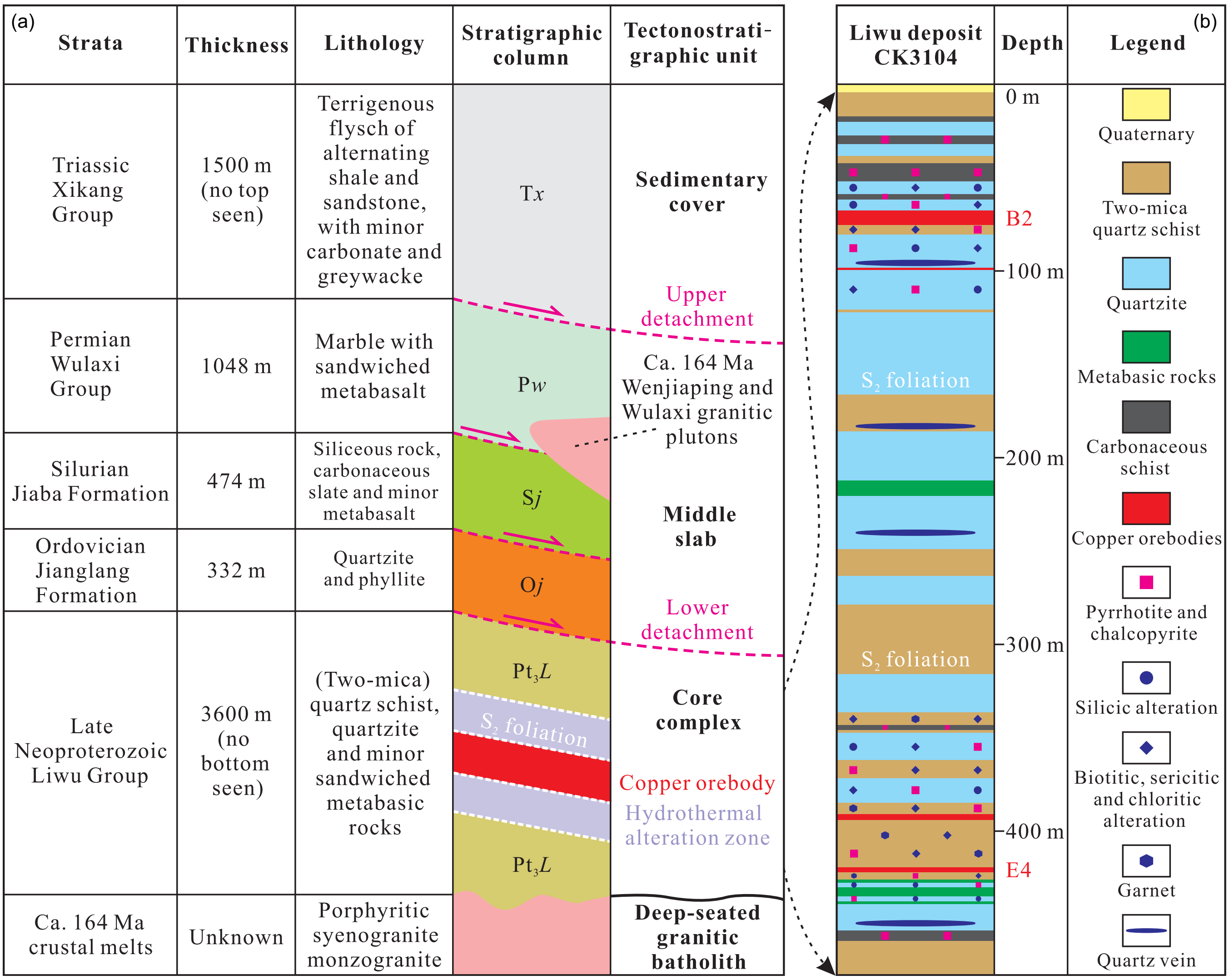

Figure 2. (a) Generalized stratigraphic column of the Jianglang Dome, modified after Yan *et al.* (2003) with the thicknesses of the geological sections we measured. (b) Column diagram of drill hole CK3104 in the Liwu deposit.

post-collisional setting during the Palaeo-Tethys Ocean closure and subsequent collision (Gao *et al.* 2023). In contrast, the late-and post-orogenic granitoids were likely associated with thickened lower crust, lithospheric delamination and asthenospheric upwelling, accompanied by extensional tectonics (Zhang *et al.* 2007).

More than ten isolated domes were distributed along the eastern Songpan-Ganze Orogen (Figure 1b), with medium-to high-grade metamorphic complexes in their cores. These domes were attributed to magma-induced uplift caused by lithospheric thermal anomalies (Yan *et al.* 1997). The Jianglang Dome consists of three tectonostratigraphic units (Figure 2a), including: (1) a core constituted by the Late Neoproterozoic Liwu Group; (2) an overlying middle slab of the Palaeozoic metamorphosed volcano-sedimentary sequences, including the Jianglang, Jiaba and Wulaxi Formations; and (3) a sedimentary cover of the Triassic Xikang Group (Yan *et al.* 1997, 2003). These units are separated by ring-like and low-angle detachment faults or ductile shear zones (Figure 1c and d).

The Neoproterozoic Liwu Group consists of a metamorphosed volcano-sedimentary sequence with a total thickness of >3600 m and is mainly composed by two-mica quartz schist, quartzite and minor (total <5 vol%) sandwiched metabasic rocks (Figure 2b). Dai *et al.* (2025a) recently dated detrital zircons and zircon xenocrysts within these rocks and assigned a Late Neoproterozoic age of ca. 544.5–538.8 Ma. The Liwu Group rocks show geochemical and Sr-Nd-Pb isotopic signatures resembling those of modern back-arc basin sediments and basalts and were most likely formed in an incipient back-arc basin along the Northern Gondwana (Dai *et al.* 2025a). Moreover, Yan *et al.* (1997) proposed that the Liwu Group suffered greenschist to amphibolite-facies metamorphism since their formation, mainly caused by ca. 525 Ma, ca. 192–184 Ma and ca. 132–121 Ma metamorphic events.

Due to multiple deformation and metamorphism, the Late Neoproterozoic Liwu Group rarely preserved its primary S_0 signs (Zhang *et al.* 2013). The S_1 foliation was possibly parallel to the S_0 layer and was commonly related to the formation of asymmetric folds. The S_1 foliation was likely associated with the Triassic compressional orogenic event in the Songpan-Ganze Orogen (Yan *et al.* 1997). The mineral assemblage consists mainly of muscovite and quartz, with minor biotite, albite, K-feldspar and garnet.

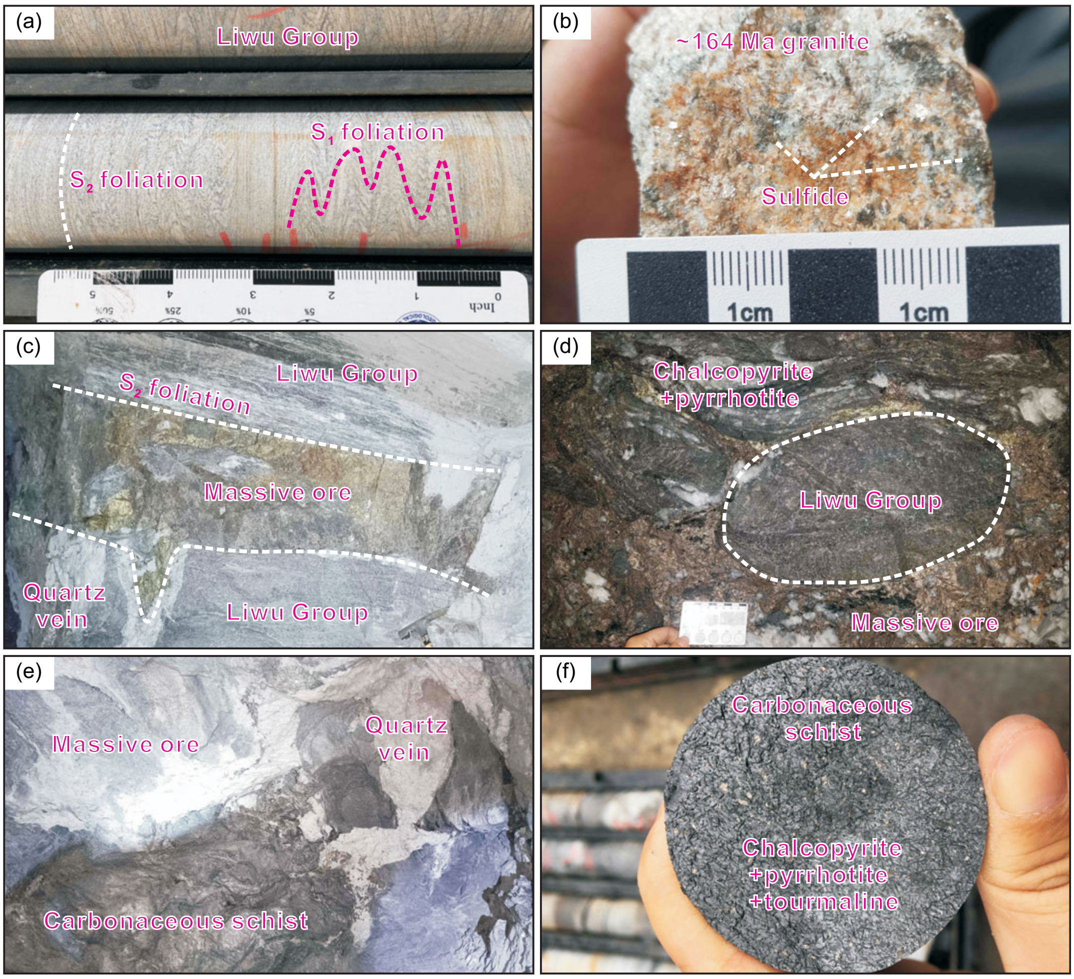

Figure 3. Field photographs of the studied stratiform Cu deposits. (a) The S1 and S2 foliation in the metasedimentary rocks of the Liwu Group. (b) Disseminated sulphides within a ca. 164 Ma granite. (c) Stratiform copper mineralization within the Liwu Group. (d) Round horsestone of the Liwu Group within massive sulphides. (e–f) Carbonaceous schist footwall rocks of Cu orebodies.

This indicates upper greenschist-facies metamorphism and yields temperatures of 300–360 °C and a pressure of 2.0×10^8 Pa based on fluid inclusion data in syntectonic quartz veins and muscovite geothermometer (Yan *et al.* 1997, 2003). The major S_2 foliation is widely developed in the Liwu Group and transposes S_1 in the field (Figure 3a). They are low-angle (20–30°) and occur as recumbent folds in some locations and were probably related to the Jurassic post-orogenic extension in the Songpan-Ganze Orogen (Roger *et al.* 2010). Their mineral assemblage is mainly composed of biotite, muscovite, quartz and garnet. This belongs to the amphibolite-facies metamorphism, with temperatures of 460–500 °C and a pressure of 3.5×10^8 Pa according to garnet-biotite and muscovite geothermometers (Yan *et al.* 1997, 2003).

The middle slab of the Jianglang Dome is composed of (1) the Ordovician Jianglang Formation mainly composed of quartzite, (2) the Silurian Jiaba Formation composed of siliceous rock, carbonaceous slate and minor metabasalt interlayers and (3) the Permian Wulaxi Formation which consists of marble and sandwiched metabasaltic rocks (Figure 2a). These strata were metamorphosed to greenschist-and amphibolite-facies during ca. 192–184 Ma and ca. 132–121 Ma metamorphism (Yan *et al.* 1997). Specifically, the Wulaxi Formation has an estimated thickness of 1048 m and was assigned a maximum depositional age of 258.9 Ma based on zircon U-Pb age and regional stratigraphic correlation (Zhu *et al.* 2020). The Triassic Xikang Group, a major component of the Songpan-Ganze Orogen, is composed of terrigenous flysch and experienced subsequent greenschist-facies metamorphism (Yan *et al.* 2003).

The Wenjiaping and Wulaxi granitic plutons are outcropping in the Jianglang Dome and its vicinity (Figure 1c and d). They intrude the Liwu Group, the Jiaba Formation and the Wulaxi Formation and occupy outcrop areas of ~34 km^2 (Wenjiaping) and ~32 km^2 (Wulaxi), respectively. In some locations, disseminated sulphides (pyrite and chalcopyrite) occur within these granites (Figure 3b). Previous studies of LA-ICP-MS zircon U-Pb dating indicate emplacement ages of 164.5 ± 0.9 Ma (Wenjiaping) and 164.3 ± 1.7 Ma (Wulaxi, Dai *et al.* 2017). Geochemical and zircon Hf isotope data suggest a post-orogenic extensional setting and a main derivation from ancient continental crust (Dai *et al.* 2017). The Wulaxi skarn-type tungsten deposit within the Permian strata is close to two granitic plutons (Figure 1c and d). It has a mineralization age of 163.7 ± 1.9 Ma according to molybdenite Re-Os dating, and a magmatic-hydrothermal origin is thus proposed for this deposit (Li *et al.* 2016). According to the geophysical studies using 1: 100, 000 gravity measurement, the core of the Jianglang Dome generally shows low residual gravity anomalies (Figure 1e),

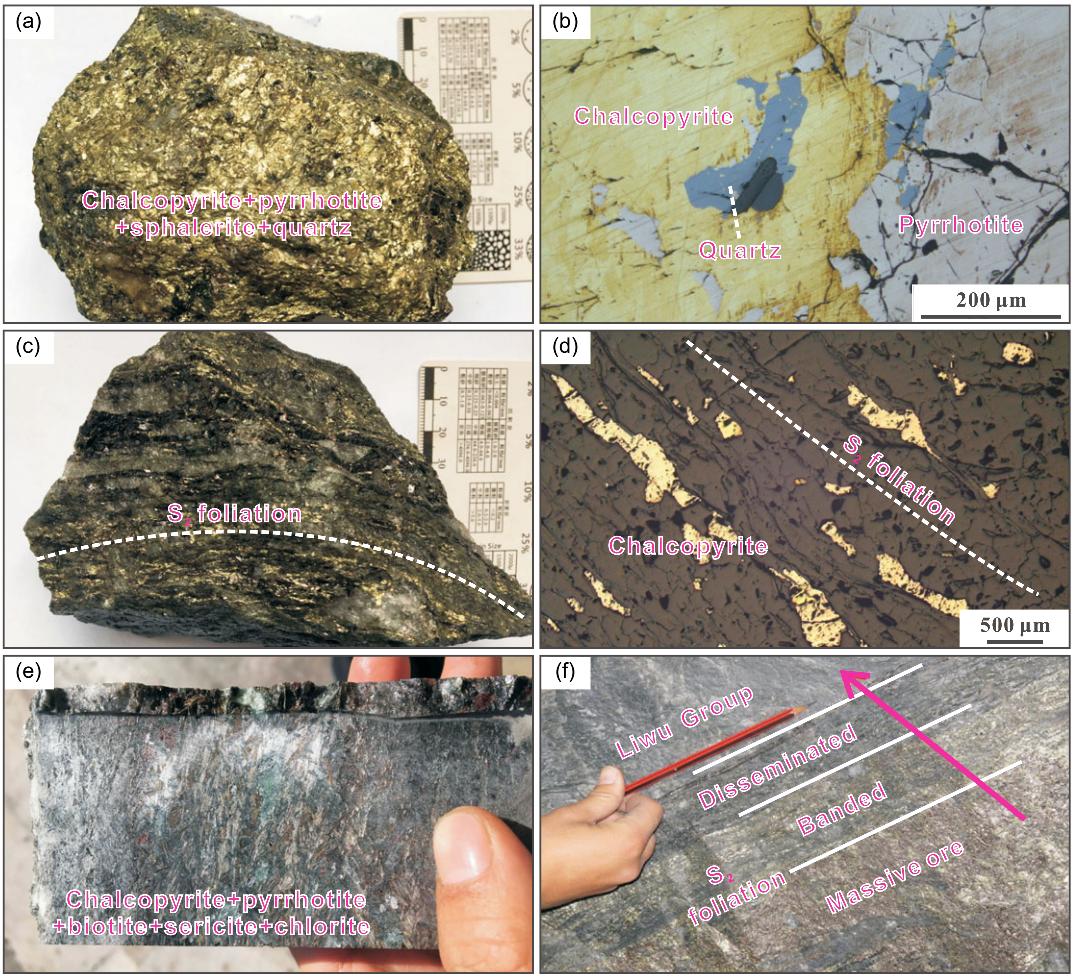

Figure 4. Field and optical microscope photographs of sulphide ores in the studied stratiform Cu deposits. (a–b) Hand specimen and microphotograph of massive sulphides. (c–d) Hand specimen and microphotograph of banded sulphides. (e) Drill core showing disseminated sulphides. (f) Gradational relationship among different ores and hosting rocks.

implying that there might be a deep-seated granitic batholith (e.g. Mangkhemthong *et al.* 2020).

2.b. Deposit geology

A series of stratiform (with minor lenticular) Cu deposits occurs within the Liwu Group in the core of the Jianglang Dome, typified by Liwu, Heiniudong and Zhongzui (Figure 1c and d). They are one of the most important copper producers in southwest China, and they have an average Cu grade of ~1.75% (up to ~20% in some places). These deposits share common characteristics in the alteration and mineralization type and are collectively referred to as 'Liwu-type' high-grade Cu deposits (Dai *et al.* 2016).

The alteration halos in these stratiform Cu deposits are roughly S_2 foliation-parallel, with thicknesses of 100–250 m from top to bottom. They are dominated by silicic, biotitic, sericitic and chloritic alteration of primary silicate minerals (Figure 2b), with an assemblage of quartz, biotite, sericite, chlorite and minor (total <10 vol%) garnet, tourmaline and staurolite. Their alteration halos generally occur along the S_2 foliation planes (Figure 2). When compared to metamorphic minerals (e.g. biotite and chlorite) in their wall rocks, these alteration minerals are present in extremely large size and high volume (Dai *et al.* 2016). The hydrothermal events can be divided into three stages according to paragenetic sequence of minerals: (1) a first stage responsible for chalcopyrite and pyrrhotite mineralization, comprising silicic (quartz), biotitic (biotite + quartz), sericitic (sericite + quartz) and chloritic (chlorite + quartz + sericite) alteration; (2) a second stage characterized by megacrystic garnet, tourmaline and staurolite; and (3) a late stage represented by non-mineralized quartz and calcite veins cross-cutting foliation.

The Cu orebodies are stratiform and lenticular within the Liwu Group (Figure 3c), locally enveloping their country rocks (Figure 3d). Mineralized and well-bedded black carbonaceous schists (2–10 m thick) are commonly distributed near the base and top of the orebodies (Figure 2b). They are mainly composed of graphite (~65 vol%), tourmaline (~15 vol%), biotite (~15 vol%), quartz (~5 vol%) and sulphide (<3 vol%). These black carbonaceous schists are smooth and easily stain hands (Figure 3e and f). Three distinct styles of sulphide mineralization with varying Cu grades have been identified in these stratiform Cu deposits: (1) massive chalcopyrite + pyrrhotite + sphalerite + pyrite + quartz, with higher Cu grades of >5% (Figure 4a and b); (2) banded chalcopyrite + pyrrhotite + quartz + biotite + sericite ± chlorite, with medium Cu grades of 1–5% (Figure 4c and d); and (3) disseminated chalcopyrite + pyrrhotite + biotite + sericite + chlorite ± quartz, with lower Cu grades of <1% (Figure 4e). From the orebody centre to its edge, three sulphide mineralization styles vary gradually (Figure 4f). This most likely indicates a paragenetic sequence of disseminated → banded → massive mineralization.

https://doi.org/10.1017/S0016756826100648 Published online by Cambridge University Press

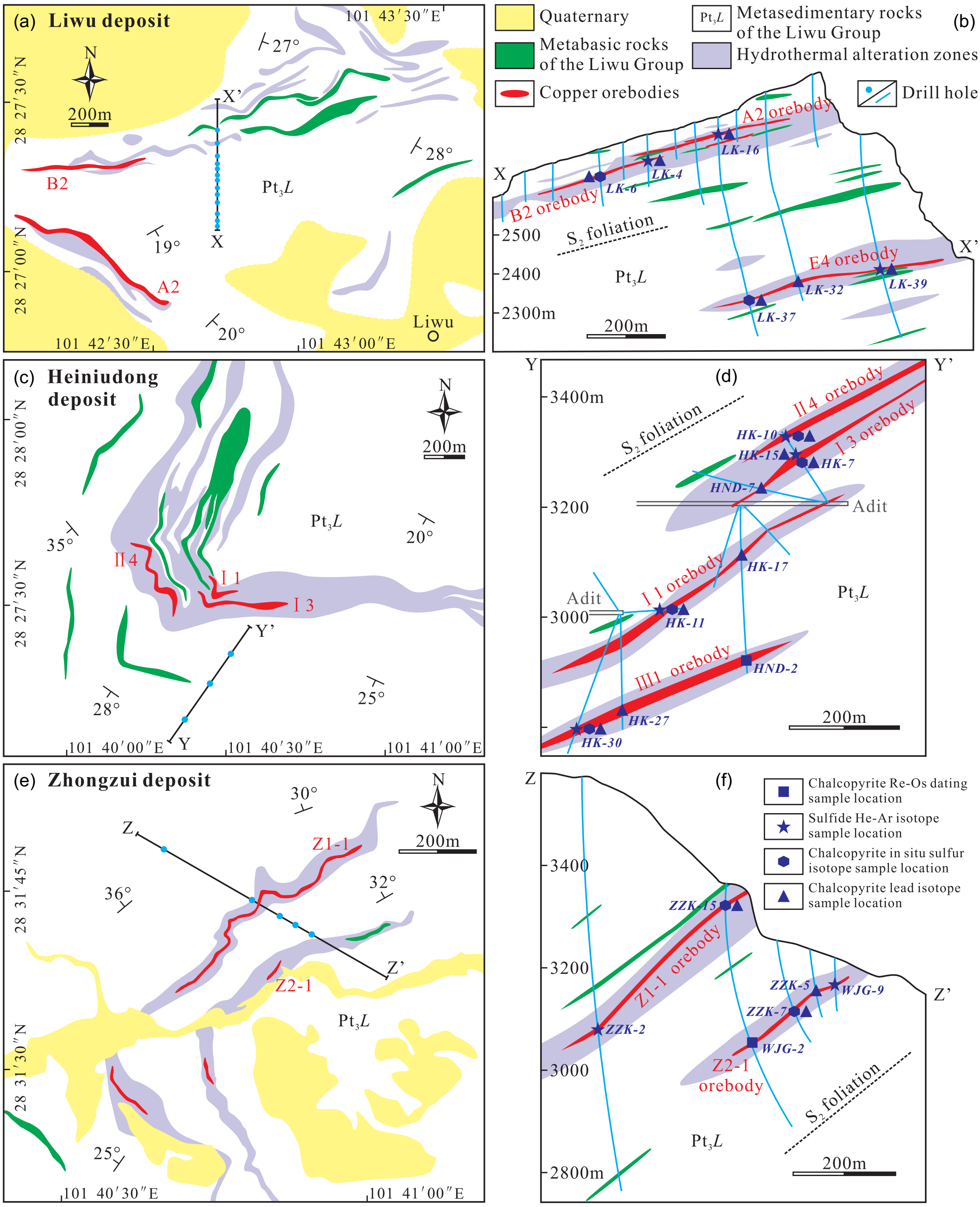

Figure 5. Geological sketch maps and cross-sections of the Liwu (a–b), Heiniudong (c–d) and Zhongzui (e–f) stratiform Cu deposits, showing some of our sample locations.

The sulphides are predominantly chalcopyrite and pyrrhotite, with minor sphalerite and pyrite. In the massive, banded and disseminated mineralization styles, the chalcopyrite grains are subhedral to anhedral, and dominantly coexisting with pyrrhotite (Figure 4b). They are commonly coarse (0.5–3 mm) in the massive ores with high chalcopyrite contents of up to 60 vol% (~20% Cu), and small (0.1–1 mm) in banded and disseminated ores (Figure 4d). Pyrrhotite is euhedral to subhedral in the massive ores, and subhedral to anhedral in the banded and disseminated ores. It is weakly magnetic and has varying pyrrhotite contents (5–60 vol% pyrrhotite) and grain sizes (0.1–2 mm). In banded and disseminated ores, the sulphides obviously occur along the S_2 foliation (Figure 4c and d). This indicates that Cu mineralization occurred earlier than or synchronously with deformation.

The Liwu, Heiniudong and Zhongzui stratiform Cu deposits are respectively located in the southeast, southwest and northwest of the Jianglang Dome (Figure 1c and d). Their Cu orebodies all occur in hydrothermal alteration halos (Figure 5). In the Liwu deposit,

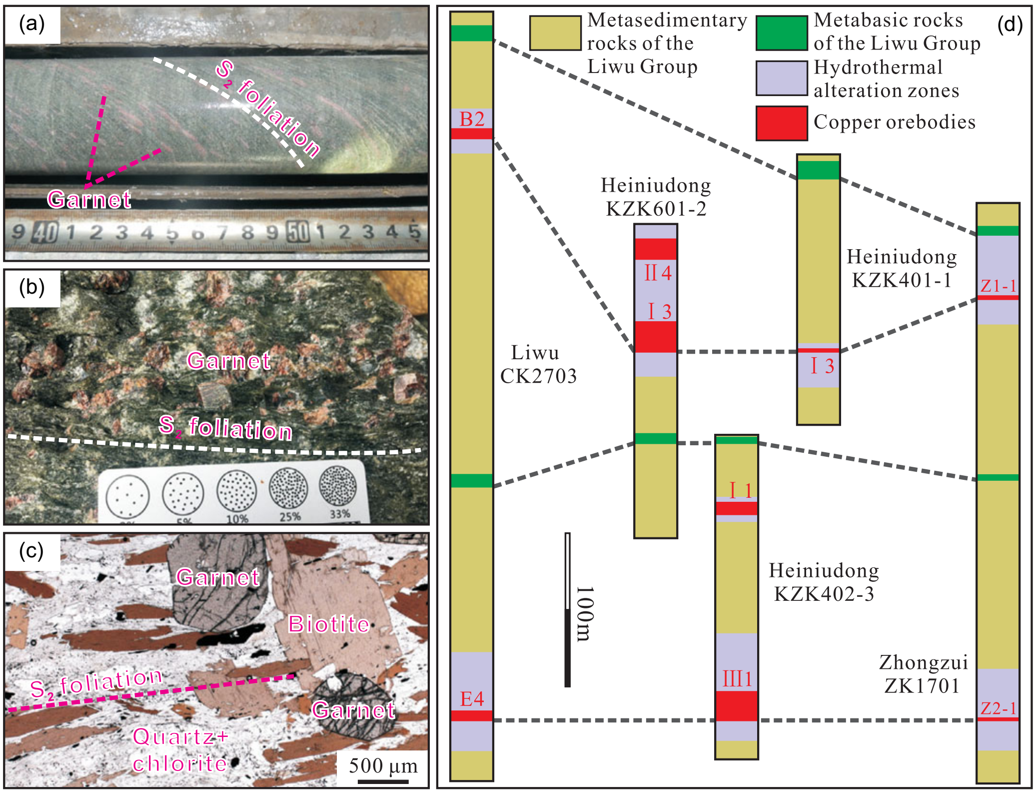

Figure 6. (a) Fine-grained deformed garnets in the shallow hydrothermal alteration parts. (b–c) Coarse-grained undeformed garnets in the deep hydrothermal alteration parts. (d) Correlation of Cu orebodies and metabasic rocks in drill cores from stratiform Cu deposits.

the Neoproterozoic Liwu Group rocks strike 20–60° and dip 19–28° SE (Figure 5a). Hydrothermal alteration zones, with a thickness of more than 200 m in some locations, can be divided into two layers (Figure 5b). The upper alteration zone contains the A2 and B2 main orebodies, extending more than 1.50 km. The lower alteration zone encloses the E4 orebody that extends ~0.5 km. In the Heiniudong deposit, the Liwu Group strikes 115–140° and dips 20–35° SW (Figure 5c). From top to bottom, four orebodies were identified based on mineral exploration (Figure 5d): (1) II4 orebody with an extension of ~250 m; (2) I3 main orebody extending more than 900 m; (3) I1 orebody with an extension of ~700 m; and (4) III1 orebody with an average thickness of ~20 m, extending more than 350 m. The Liwu Group rocks in the Zhongzui deposit area strike 35–70° and dip 25–36° NW (Figure 5e). Two hydrothermal alteration envelopes were discovered based on geologic mapping and drill cores. They contain stratiform orebodies, including the upper Z1-1 orebody with an extension of >3.50 km and the lower Z2-1 orebody extending ~1.0 km (Figure 5f).

According to field observations, fine-grained (<5 mm) garnets are widely distributed in the shallower hydrothermal alteration halos, which host the A2 and B2 orebodies of Liwu, the II4, I3 and I1 orebodies of Heiniudong and the Z1-1 orebody of Zhongzui (Figure 5). These fine-grained garnets are commonly elongated and deformed and are S_2 foliation-parallel (Figure 6a). In contrast, coarse-grained (up to 25 mm) garnets occur in the deep hydrothermal alteration zones, which contain the E4 orebody of Liwu, the III1 orebody of Heiniudong and the Z2-1 orebody of Zhongzui (Figure 5). These undeformed and coarse-grained garnets are present as phenocrysts (Figure 6b and c) and are absent in the shallower parts. In addition, the available exploration information indicates a similar altitude difference of ~200 m between the deep and shallow orebodies (Figure 6d). Further, several metabasic rocks can also be connected at the same altitudes. In conjunction, the deep and the shallow orebodies each belong to the same layer in the Jianglang Dome (Figure 6d), indicating that they can be fitted together and occur in a narrow stratigraphic range (Dai *et al.* 2025b). Recent geological mapping shows that the hydrothermal alteration zones with thicknesses of 100–250 m are stably and annularly distributed on the surface (Figure 1c and d), implying significant exploration potential in this region.

2.c. Sample description

We collected massive and banded ore samples with weights of 1–3 kg from the Liwu, Heiniudong and Zhongzui stratiform Cu deposits, as well as ca. 164 Ma Wenjiaping and Wulaxi granite samples in the Jianglang Dome. Their sample locations are listed in Supplementary Tables S1–S4 and are partially marked in Figure 1c and Figure 5. Disseminated ores were not sampled, because they only have a small amount of sulphide minerals. All ore samples were crushed and then sieved with the #80 mesh (180 µm) for mineral separation. Chalcopyrite and pyrrhotite grains were separated using conventional LST heavy liquids and magnetic techniques, and then they were hand-picked under a binocular microscope at the Regional Geological Survey Institute of Hebei Province (Geotourism Research Center of Hebei Province), Langfang, China. Granite samples ($n = 4$) were crushed into 200 mesh (75 µm) for whole-rock Pb isotopic measurements.

The massive ore samples (e.g. Re-Os sample WJG-2 and He-Ar sample LK-16) are mainly composed of chalcopyrite (15–45 vol%), pyrrhotite (10–60 vol%), quartz (5–30 vol%), sphalerite (0–10 vol %) and pyrite (0–5 vol%). The banded varieties (e.g. Re-Os sample HND-2 and He-Ar sample LK-39) mainly comprise chalcopyrite (3–15 vol%), pyrrhotite (2–20 vol%) and extensive gangue minerals (65–95 vol%, such as quartz, biotite, sericite and chlorite). In

https://doi.org/10.1017/S0016756826100648 Published online by Cambridge University Press

this study, three chalcopyrite separates within massive and banded ores were sampled for Re-Os dating. Nineteen chalcopyrite and one pyrrhotite samples from different Cu orebodies were used for He-Ar isotopes of fluid inclusions, and eighteen polished sections of ores were chosen for chalcopyrite in situ S isotopes. Moreover, chalcopyrite grains from forty massive and banded ore samples were selected for Pb isotopes. Detailed sampling locations and analytical results are available in Supplementary Tables S1–S4.

Granite samples were collected from the Wenjiaping and Wulaxi plutons (Figure 1c). They show a typical porphyritic texture with ~20 vol% K-feldspar phenocryst (1.0–2.5 mm), as well as ~40 vol% quartz, ~25 vol% K-feldspar, ~10 vol% biotite and ~5 vol % sericite groundmass. In this study, Pb isotope measurements were conducted on four granite samples for comparison (Supplementary Tables S4).

3. Analytical methods

Chalcopyrite Re-Os dating was performed at the National Research Center of Geoanalysis, Chinese Academy of Geological Sciences. All samples were dissolved using the Carius tube method described by Shirey and Walker (1995). Re was recovered by ion exchange, and Os was recovered by distilling the sample solution and then purified by micro-distillation. Their concentrations and isotope ratios were determined using negative thermal ionization mass spectrometry. The blank sample BK yielded extremely low Re (0.0018 ± 0.0001 ppb), Os (0.00026 ± 0.00001 ppb) and ^{187}Os (0.000012 ± 0.000002 ppb) concentrations. The chalcopyrite standard GBW04477/JCBY was used to control reproducibility and instrument stability (Du *et al.* 2012), and detailed analytical procedures followed those in Du *et al.* (2004). Re-Os isochron ages were calculated with 2σ uncertainty using the online IsoplotR programme (Vermeesch, 2018).

Sulphide He-Ar isotopic analysis was conducted with a one-step crushing technique at the Institute of Geology and Geophysics, Chinese Academy of Sciences. The crusher was constructed from 316L stainless steel, and noble gas isotope analyses were performed on a Noblesse mass spectrometer in static mode. The detailed crushing and analytical procedures were described by He *et al.* (2011). Helium blanks were negligible (^{3}He blank < 3×10^{-17} cm^3 STP); Ar blanks were small, about 0.1% relative to the signals. The air standard, with ^{3}He/^{4}He ratio of 1.384 × 10^{-6} (Ra) and ^{40}Ar/^{36}Ar ratio of 298.5, was measured every two weeks. The uncertainty of the average ^{3}He/^{4}He ratio of calibration measurements is better than 5%. Thus, 5% error was assigned to the calculated ^{3}He/^{4}He ratio, and this error was included in the unknown sample correction. The results were normalized to the value of the air standard and corrected for system blanks.

In situ sulphur isotope analyses of chalcopyrite were carried out on a Neptune Plus MC-ICP-MS (Thermo Fisher Scientific, Bremen, Germany) equipped with a Geolas HD excimer ArF laser ablation system (Coherent, Göttingen, Germany) at the Wuhan Sample Solution Analytical Technology Co., Ltd, Hubei, China. Helium was used as the carrier gas for the ablation cell and was mixed with argon after the ablation cell. The single spot ablation mode was used, and then the large spot size (44 μm) and slow pulse frequency (2 Hz) were used to avoid the downhole fractionation effect (Fu *et al.* 2016). To avoid the matrix effect, a chalcopyrite standard GBW07268 (a pressed pellet, $\delta^{34}S_{V\text{-}CDT}$ = −0.30 ± 0.27, Fu *et al.* 2016) was chosen as a reference material, which yielded consistent $\delta^{34}S_{V\text{-}CDT}$ values of −0.302 ± 0.028 (n = 15, mean square of weighted deviates [MSWD] = 1.2).

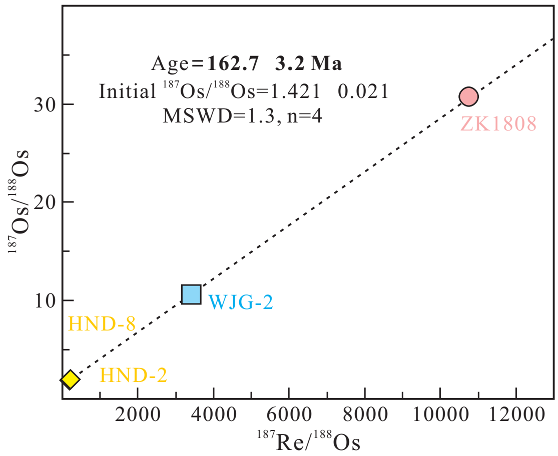

Figure 7. Chalcopyrite Re-Os isochron age for the stratiform Cu deposits. MSWD = mean square of weighted deviates, a measure of scatter. Data of sample ZK1808 from Zhou *et al.* (2017).

Lead isotope analysis is carried out at the Nanjing FocuMS Technology Co. Ltd, using Agilent Technologies 7700x quadrupole ICP-MS (Hachioji, Tokyo, Japan) to determine the exact contents of Pb available. Diluted solution (40 ppb Pb doping with 10 ppb Tl) was introduced into Nu Instruments Nu Plasma II MC-ICP-MS (Wrexham, Wales, UK) by Teledyne Cetac Technologies Aridus II desolvating nebulizer system (Omaha, Nebraska, USA). Raw data of Pb isotope ratios were corrected for mass fractionation by normalizing to ^{205}Tl/^{203}Tl = 2.3885 with the exponential law. Isotopic standard NIST981 was periodically analysed to correct instrumental drift, and geochemical reference materials BCR-2, BHVO-2, AVG-2, RGM-2 (Weis *et al.* 2006) were treated as quality control.

4. Results

4.a. Chalcopyrite Re-Os dating

Three chalcopyrite separates in this paper, as well as sample ZK1808 in Zhou *et al.* (2017), were selected from the Heiniudong and Zhongzui deposits (Figure 5d and f). Four chalcopyrite samples show variable Re (0.3411–1.6931 ppb) and Os (0.00070–0.03731 ppb) concentrations. They yield ^{187}Re/^{188}Os ratios of 194–10700 and ^{187}Os/^{188}Os ratios of 1.958–30.70 (Supplementary Table S1). Together, data points yield an isochron date of 162.7 ± 3.2 Ma and an initial ^{187}Os/^{188}Os ratio of 1.421 ± 0.021 (2σ, n = 4, MSWD = 1.3, Figure 7).

4.b. Sulphide He-Ar isotopes

The He-Ar isotope results of fluid inclusions within chalcopyrite (n = 19) and pyrrhotite (n = 1) are listed in Supplementary Table S2. These samples have ^{4}He contents of 1.34–47.18 × 10^{-7} ccSTP/g, ^{40}Ar contents of 0.17–18.71 × 10^{-7} ccSTP/g and ^{40}Ar* contents of 0.10–7.80 × 10^{-7} ccSTP/g, respectively. They show variable R/Ra ratios of 0.052–0.144 [R/Ra = $(^3He/^4He)_{sample}/(^3He/^4He)_{air}$, where $(^3He/^4He)_{air}$ is actual measurement data in this study], ^{40}Ar/^{36}Ar ratios of 479–2463 and ^{40}Ar*/^{4}He ratios of 0.013–0.804.

The calculated F^{4}He values [F^{4}He = $(^4He/^{36}Ar)_{sample}/(^4He/^{36}Ar)_{air}$, where $(^4He/^{36}Ar)_{air}$ = 0.1655, Kendrick *et al.* 2001] for our sulphide samples give ranges of 1600–474417. They have He_{mantle} values of 0.69–2.20 wt.% {He_{mantle} (%) = [$(^3He/^4He)_{sample}$ – (^{3}He/

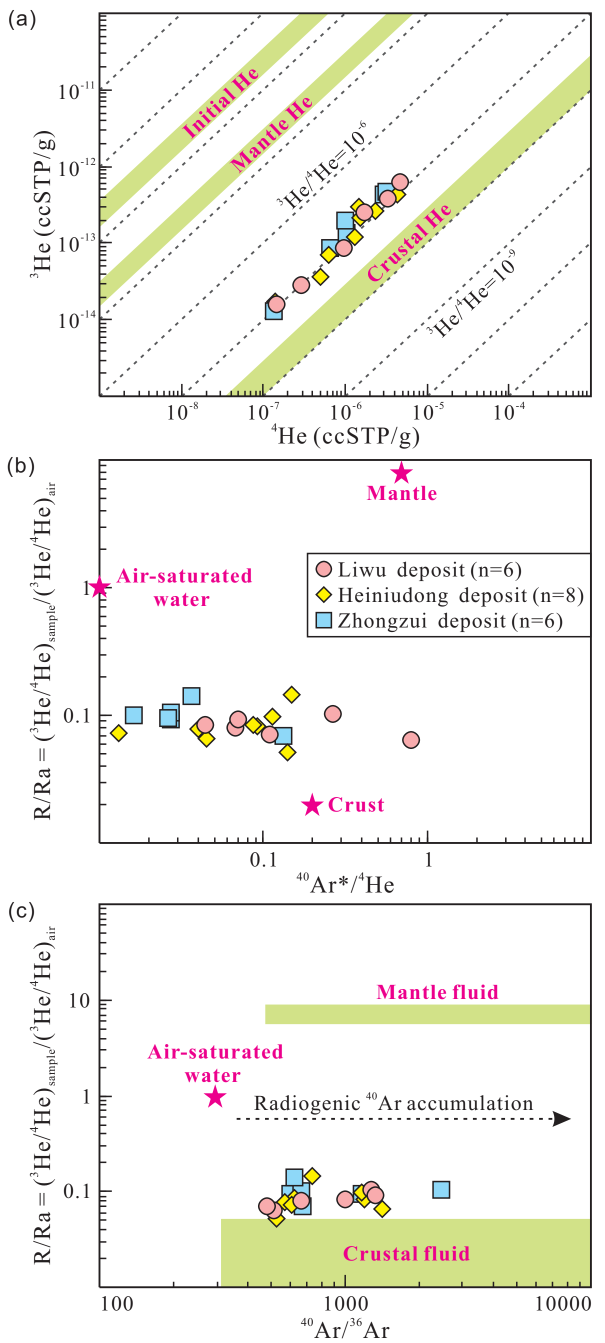

Figure 8. He-Ar isotope composition of chalcopyrite from stratiform Cu deposits. (a) ^{4}He versus ^{3}He diagram, the ^{3}He/^{4}He ratios and fields of initial He, mantle He, and crustal He are from Mamyrin and Tolstikhin (1984). (b) ^{40}Ar*/^{4}He versus R/Ra diagram, the data of crust (R/Ra = 0.02, ^{40}Ar*/^{4}He = 0.2) and mantle (R/Ra = 8, ^{40}Ar*/^{4}He = 0.69 ± 0.06) are from Ballentine *et al.* (2002), and the data of air-saturated water after Stuart *et al.* (1995). (c) ^{40}Ar/^{36}He versus R/Ra diagram, the fields of mantle and crustal fluids from Hu *et al.* (2009).

^{4}He)$_{crust}$]/[(^{3}He/^{4}He)$_{mantle}$ − (^{3}He/^{4}He)$_{crust}$] × 100, where (^{3}He/^{4}He)$_{crust}$ = 0.01 Ra and (^{3}He/^{4}He)$_{mantle}$ = 6.1 Ra, Stuart *et al.* 1995; Gautheron and Moreira, 2002}. On the ^{4}He versus ^{3}He, ^{40}Ar*/^{4}He versus R/Ra, and ^{40}Ar/^{36}He versus R/Ra diagrams, all the sulphide samples plot near the field of crustal He and fluid, with insignificant mantle signatures (Figure 8a, b and c). This indicates that the ore-forming fluids were dominantly derived from a crustal source.

4.c. Chalcopyrite in situ S isotopes

Chalcopyrite in situ S isotope data ($n = 72$) are provided in Supplementary Table S3. Several measurements conducted on individual chalcopyrite grains indicate that their internal sulphur isotopic compositions are homogeneous (Figure 9a and b). In general, our analysed spots display a $\delta^{34}S_{V\text{-}CDT}$ (Vienna-Canyon Diablo Troilite) range from 3.87‰ to 9.50‰ (Figure 9c). These data are compatible with $\delta^{34}S_{V\text{-}CDT}$ values of chalcopyrite and pyrrhotite separates in the Jianglang Dome (5.6–8.7‰, Yan *et al.* 1997). These positive $\delta^{34}S_{V\text{-}CDT}$ determinations are comparable to those of magnetite-series granitoids ($\delta^{34}S_{V\text{-}CDT}$ = 1–9‰), which were thought to originate from dominantly igneous protoliths (Sasaki and Ishihara, 1979; Seal, 2006). This matches the I-type affinity of the Wenjiaping and Wulaxi granite in the Jianglang Dome (Dai *et al.* 2017).

4.d. Chalcopyrite and granite Pb isotopes

Lead isotope compositions of chalcopyrite separates ($n = 40$) have ^{206}Pb/^{204}Pb ratios of 18.0252–19.6826, ^{207}Pb/^{204}Pb ratios of 15.6857–15.7943 and ^{208}Pb/^{204}Pb ratios of 38.2784–40.5011, respectively (Supplementary Table S4). Samples HK-8, HK-20, HK-27, ZZK-5 and ZZK-7 have relatively high lead isotope values, e.g. ^{206}Pb/^{204}Pb ratios of 18.6683–19.6826, ^{207}Pb/^{204}Pb ratios of 15.7579–15.7943 and ^{208}Pb/^{204}Pb ratios of 39.2542–40.5011. The others show homogeneous isotope composition and do not vary significantly with mineralization types. They exhibit ^{206}Pb/^{204}Pb ratios of 18.0252–18.5496, ^{207}Pb/^{204}Pb ratios of 15.6857–15.7817 and ^{208}Pb/^{204}Pb ratios of 38.2784–39.0836 ($n = 35$). These data broadly match those of ca. 164 Ma Wenjiaping ($n = 2$) and Wulaxi ($n = 2$) granites, with ^{206}Pb/^{204}Pb ratios of 18.6507–18.9474, ^{207}Pb/^{204}Pb ratios of 15.6794–15.7415 and ^{208}Pb/^{204}Pb ratios of 38.9631–39.2406. According to the ^{206}Pb/^{204}Pb versus ^{207}Pb/^{204}Pb (Zartman and Doe, 1981) and Δβ versus Δγ diagrams {$\Delta\beta = [(^{207}Pb/^{204}Pb)_{common}/(^{207}Pb/^{204}Pb)_{mantle} - 1] \times 1000$, $\Delta\gamma = [(^{208}Pb/^{204}Pb)_{common}/(^{208}Pb/^{204}Pb)_{mantle} - 1] \times 1000$, where $(^{207}Pb/^{204}Pb)_{mantle} = 15.43$, $(^{208}Pb/^{204}Pb)_{mantle} = 37.63$, Zhu, 1998}, upper crust-derived lead components are preferred for the investigated chalcopyrite grains and associated granitic rocks (Figure 10a and b).

5. Discussion

5.a. Epigenetic magmatic-hydrothermal mineralization

Chalcopyrite Re-Os chronometers are widely used to date mineralization events of sulphide deposits, and their high closure temperatures (> 500 °C, Zhu and Sun, 2013) could prevent isotopic disturbance in the absence of sulphide recrystallization (e.g. Muchez *et al.* 2015). For example, Zhu and Sun (2013) studied the Lala deposit in the Kangdian copper belt, southwestern China, and suggested that chalcopyrite Re-Os systematics were almost unaffected by metamorphic temperatures up to 500 °C. Previous studies indicated multiple deformation and metamorphism for the Late Neoproterozoic Liwu Group: (1) upper greenschist-facies likely attributed to the Triassic orogenic event, with temperatures of 300–360 °C based on fluid inclusion data and muscovite geothermometer; and (2) amphibolite-facies probably related to the Jurassic post-orogenic extension, with temperatures of 460–500 °C based on garnet-biotite and muscovite geothermometers (Yan *et al.* 1997, 2003). These metamorphic temperatures are obviously

https://doi.org/10.1017/S0016756826100648 Published online by Cambridge University Press

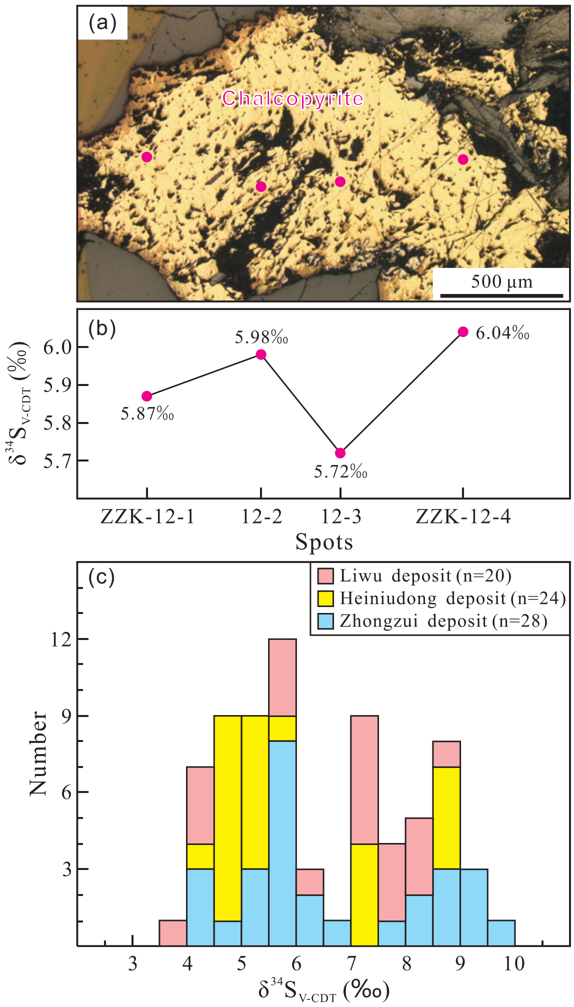

Figure 9. (a–b) Representative section of in situ sulphur isotope in individual chalcopyrite grains. (c) Sulphur isotope histogram of chalcopyrite from stratiform Cu deposits in the Jianglang Dome.

lower than the closure temperatures of chalcopyrite Re-Os chronometers (> 500 °C, Zhu and Sun, 2013).

In this study, chalcopyrite Re-Os geochronology was used to constrain the Cu mineralization age in the Liwu Group. Four samples yield an isochron age of 162.7 ± 3.2 Ma (2σ, $n = 4$, MSWD = 1.3, Figure 7), and place a best estimate for epigenetic mineralization age. This is equivalent to the previous chalcopyrite Re-Os age of stratiform Cu deposits in the Jianglang Dome (161.8 ± 2.5 Ma, Dai *et al.* 2025b), molybdenite Re-Os age of the Wulaxi skarn-type tungsten deposit (163.7 ± 1.9 Ma, Li *et al.* 2016), as well as zircon U-Pb ages of the Wenjiaping and Wulaxi granitic plutons (164.5–164.3 Ma, Dai *et al.* 2017). Besides, Zhou *et al.* (2017) obtained a chalcopyrite Re-Os isochron age of 151.1 ± 4.8 Ma (2σ, $n = 5$, MSWD = 5.8) for the Liwu and Zhongzui deposits, and suggested a post-magmatic hydrothermal origin. However, our new isochron age is more robust with much lower MSWD (mean square of weighted deviates) values, most likely indicating a magmatic-hydrothermal affinity.

The initial $^{187}Os/^{188}Os$ ratio (1.421 ± 0.021, Figure 7) is comparable to that of the upper continental crust (1.4–1.9, Peucker-Ehrenbrink and Jahn, 2001), and thus suggests a crustal origin. Recent studies showed that fresh metabasic and metasedimentary rocks of the Liwu Group are metalliferous with an average Cu content of 93.3 ppm (Dai *et al.* 2025a), much higher than the continental upper crust (Cu = 25 ppm, Taylor and McLennan, 1985). Besides, chalcopyrite Re-Os dating yielded an isochron age of 549 ± 11 Ma (2σ, $n = 5$, MSWD = 15) for massive ores of the Liwu, Heiniudong and Zhongzui deposits, indicating syngenetic mineralization (Dai *et al.* 2025a). All these data confirm two-staged formation of ca. 549 Ma syngenetic enrichment overprinted by ca. 163 Ma epigenetic magmatic-hydrothermal mineralization, for the stratiform Cu deposits hosted by the Late Neoproterozoic (ca. 544.5–538.8 Ma) Liwu Group.

Throughout the whole Songpan-Ganze Orogen, medium-pressure Barrovian-type metamorphism was initiated at ca. 210–205 Ma due to crustal thickening and shortening, and peak metamorphism with temperatures of 410–530 °C was recorded at ca. 204–190 Ma according to monazite U-Pb and garnet Sm-Nd ages (Huang *et al.* 2003a, 2003b). More recently, Dai *et al.* (2025b) dated metamorphic monazites within two-mica quartz schist from the Zhongzui deposit of the Jianglang Dome, and obtained a weighted mean $^{206}Pb/^{238}U$ age of 193.0 ± 1.1 Ma ($n = 25$, MSWD = 2.0). This is attributed to ca. 204–190 Ma peak metamorphism in the Songpan-Ganze Orogen, which predates ca. 163 Ma epigenetic mineralization within the Liwu Group by a large time span. Besides, synorogenic metamorphic fluids typically produce widespread deposits (e.g. Perelló *et al.* 2015; Qiu *et al.* 2021), yet large-scale Cu deposits remain hitherto unique in the Songpan-Ganze Orogen. Thus, this evidence indicates that epigenetic Cu mineralization in the Jianglang Dome was unlikely to be associated with synorogenic metamorphic fluids, which were commonly formed during prograde metamorphism. Further, the Triassic compressional orogenic event in the Songpan-Ganze Orogen likely formed the S_1 foliation in the Liwu Group rocks (Yan *et al.* 1997, 2003), which was locally overprinted and transposed by the S_2 foliation (Figure 3a) due to the Jurassic post-orogenic extension in the Songpan-Ganze Orogen (Roger *et al.* 2010).

5.b. Coupled source signatures of fluids and metals

As noted above, previous studies have conducted sulphur isotope on sulphides (Yan *et al.* 1997) and boron isotope on ore-associated tourmalines (Zhou *et al.* 2017) and indicated a magmatic-hydrothermal affinity for stratiform Cu deposits in the Jianglang Dome. However, quantitative contributions of crustal (e.g. felsic basement rocks and ca. 164 Ma granites) or mantle-derived (e.g. mafic basement rocks) components of the ore-forming fluids remain unknown.

Sulphide minerals could effectively retain He, and their He-Ar isotopes are sensitive to tracing the ore-forming fluid sources (Hu *et al.* 2009; Goodwin *et al.* 2017). Previous studies have shown significant variation in R/Ra ratios for fluids derived from different geological reservoirs [$R/Ra = (^3He/^4He)_{sample}/(^3He/^4He)_{air}$, where $(^3He/^4He)_{air} = 1.39 \times 10^{-6}$ (Stuart *et al.* 1995) and are actual measurement data in Supplementary Table S2], e.g. air-saturated water of 1, continental crust of 0.01–0.05 and subcontinental lithospheric mantle of 6.1 (Stuart *et al.* 1995; Gautheron and Moreira, 2002). In this paper, fluid inclusions within chalcopyrite and pyrrhotite show low R/Ra ratios of 0.052–0.144, indicating a dominantly crustal origin with negligible mantle-derived inputs. This is further illuminated by diverse discriminant diagrams (Figure 8a, b and c) and calculated He_{mantle} values of 0.69–2.20 wt.% (Supplementary Table S2). Interestingly, the He_{mantle} values match the proportion of sandwiched metabasic rocks in the Liwu

https://doi.org/10.1017/S0016756826100648 Published online by Cambridge University Press

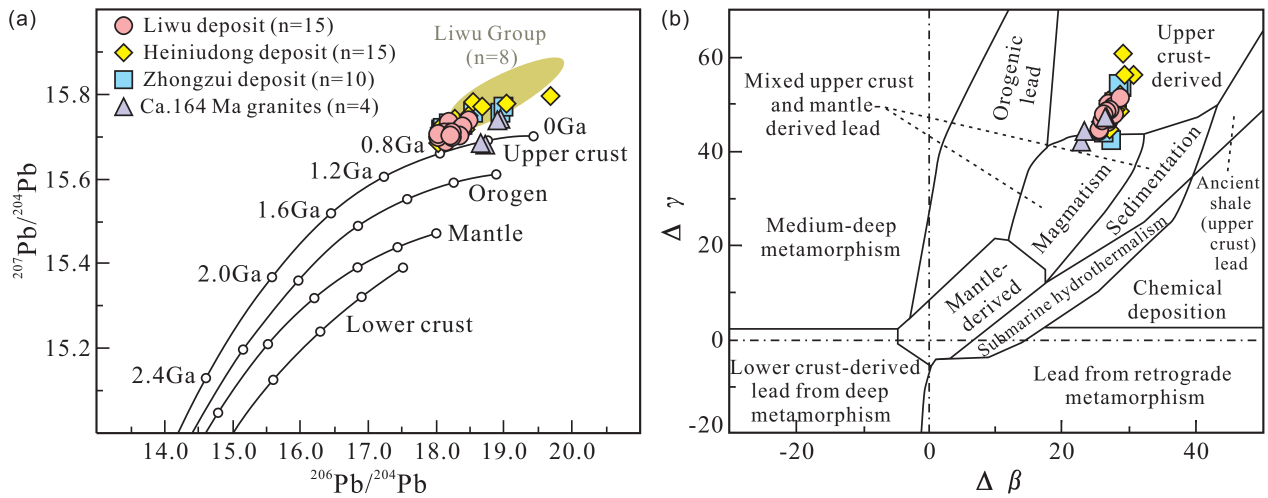

Figure 10. (a) Plot of $^{206}Pb/^{204}Pb$ versus $^{207}Pb/^{204}Pb$ for chalcopyrite separates and ca. 164 Ma granites (based on Zartman and Doe, 1981), the data of the Liwu Group rocks after Dai *et al.* (2025a). (b) Δβ versus Δγ diagram of lead isotopes (based on Zhu, 1998), $\Delta\beta = [(^{207}Pb/^{204}Pb)_{common}/(^{207}Pb/^{204}Pb)_{mantle} - 1] \times 1000$, $\Delta\gamma = [(^{208}Pb/^{204}Pb)_{common}/(^{208}Pb/^{204}Pb)_{mantle} - 1] \times 1000$, where $(^{207}Pb/^{204}Pb)_{mantle} = 15.43$, $(^{208}Pb/^{204}Pb)_{mantle} = 37.63$.

Group (total <5 vol%), which are most likely responsible for minor mantle contribution during the epigenetic mineralization event. Besides, the measured $^{40}Ar/^{36}Ar$ ratios range from 479 to 2463, much higher than modern atmospheric values ($^{40}Ar/^{36}Ar = 295.5$, Steiger and Jäger, 1977). This is attributed to significantly high concentration of $^{40}Ar^*$ (radiogenic ^{40}Ar) of crustal sources, which could be estimated using the measured maximum $^{40}Ar/^{36}Ar$ values of sulphide samples as follows (Kendrick *et al.* 2001): $^{40}Ar^* (\%) = \{([^{40}Ar/^{36}Ar)_{max} - 295.5] \times 100\}/(^{40}Ar/^{36}Ar)_{max}$. The calculated maximum $^{40}Ar^*$ concentration for the studied stratiform Cu deposits is 88%, indicating more than 88% of $^{40}Ar/^{36}Ar$ values were derived from crustal sources (e.g. Cao *et al.* 2015). Besides, their $^{40}Ar^*/^{4}He$ ratios vary between 0.013 and 0.263 (except 0.804 of sample LK-39, Supplementary Table S2), resembling the crustal ratio of 0.2 and much lower than the mantle value of 0.69 ± 0.06 (Ballentine *et al.* 2002). This seems more likely to be associated with the involvement of air-saturated water, which could reduce $^{40}Ar^*/^{4}He$ ratios and elevate R/Ra values of the crustal ore-forming fluids (Figure 8b and c). Further, atmospheric He contribution can be detected by the F^4He value, which is defined as $^{4}He/^{36}Ar$ of a sample relative to the atmospheric $^{4}He/^{36}Ar$ value (0.1655, Kendrick *et al.* 2001). However, the calculated F^4He values for our sulphide samples are all more than 1600, which indicates a minor contribution of atmospheric He ($F^4He = 1$) that could be sucked into air-saturated water (Cao *et al.* 2015). Synthetically, He-Ar isotope data of fluid inclusions within chalcopyrite and pyrrhotite separates suggest that the ore-forming fluids were dominated by crustal origin, with minor air-saturated water and negligible (0.69–2.20 wt.%) mantle components.

The sulphur isotope ratio of sulphides was widely used to trace the sources of sulphur and ore-forming fluids (e.g. Seal, 2006; Guo *et al.* 2024). However, traditional sulphur isotope measurement obtains an average value of a whole-rock sample and masks possible isotopic heterogeneity between individual minerals. In this contribution, several in situ S isotope sections on individual chalcopyrite grains reveal uniform sulphur isotopic compositions (Figure 9a and b). All the analysed chalcopyrite grains yield $\delta^{34}S_{V\text{-}CDT}$ values between 3.87–9.50‰ (Figure 9c, Supplementary Table S3) and are consistent with previous results of chalcopyrite and pyrrhotite separates ($\delta^{34}S_{V\text{-}CDT} = 5.6–8.7‰$, Yan *et al.* 1997). These data can be attributed to their genetic affinity with magnetite-series granitoids, which have positive $\delta^{34}S_{V\text{-}CDT}$ values of 1–9‰ and were derived from dominantly igneous protoliths (Sasaki and Ishihara, 1979; Seal, 2006). Based on petrological and geochemical studies, Dai *et al.* (2017) proposed an I-type affinity for the Wenjiaping and Wulaxi granites in the Jianglang Dome, caused by partial melting of igneous source rocks. This likely induced all positive $\delta^{34}S_{V\text{-}CDT}$ values of chalcopyrite (3.87–9.50‰) from the stratiform Cu deposits in this region.

Lead isotopes are useful in evaluating the metal sources and the nature of lead reservoirs (Zartman and Doe, 1981; Zhu, 1998). The measured chalcopyrite separates within sulphide ores are characterized by variable Pb isotope compositions, with $^{206}Pb/^{204}Pb$ ratios of 18.0252–19.6826, $^{207}Pb/^{204}Pb$ ratios of 15.6857–15.7943 and $^{208}Pb/^{204}Pb$ ratios of 38.2784–40.5011 ($n = 40$, Supplementary Table S4). These data broadly match values of regional granites, with $^{206}Pb/^{204}Pb$ ratios of 18.6507–18.9474, $^{207}Pb/^{204}Pb$ ratios of 15.6794–15.7415 and $^{208}Pb/^{204}Pb$ ratios of 38.9631–39.2406 ($n = 4$). On the $^{206}Pb/^{204}Pb$ versus $^{207}Pb/^{204}Pb$ diagram, all the chalcopyrite and granite samples are close to the defined upper crust growth curve and the Pb isotope field of the Liwu Group rocks (Figure 10a). On the Δβ versus Δγ diagram, their data points are plotted in the upper crust-derived and magmatism domains (Figure 10b). All these Pb isotope features indicate that most of the lead came from the upper crust, showing a genetic affinity with ca. 164 Ma granites and the Late Neoproterozoic Liwu Group rocks.

Combined with geochronological, geochemical and isotopic data in this study and Dai *et al.* (2017, 2025b), we propose that both ca. 164 Ma crust-derived granitic magmatism and the fertile Liwu Group rocks contributed significantly to the ore metal budget in the Jianglang Dome. During magma ascent processes, the crustal melts might be contaminated by the metalliferous Liwu Group, inducing similar Pb isotope signatures (Figure 10a) and sulphide-bearing granite in some locations (Figure 3b).

5.c. Mineralization potential and genetic model

All the robust geochronological and isotopic evidence presented above confirms an epigenetic magmatic-hydrothermal mineralization at ca. 163 Ma for the investigated stratiform Cu deposits in

https://doi.org/10.1017/S0016756826100648 Published online by Cambridge University Press

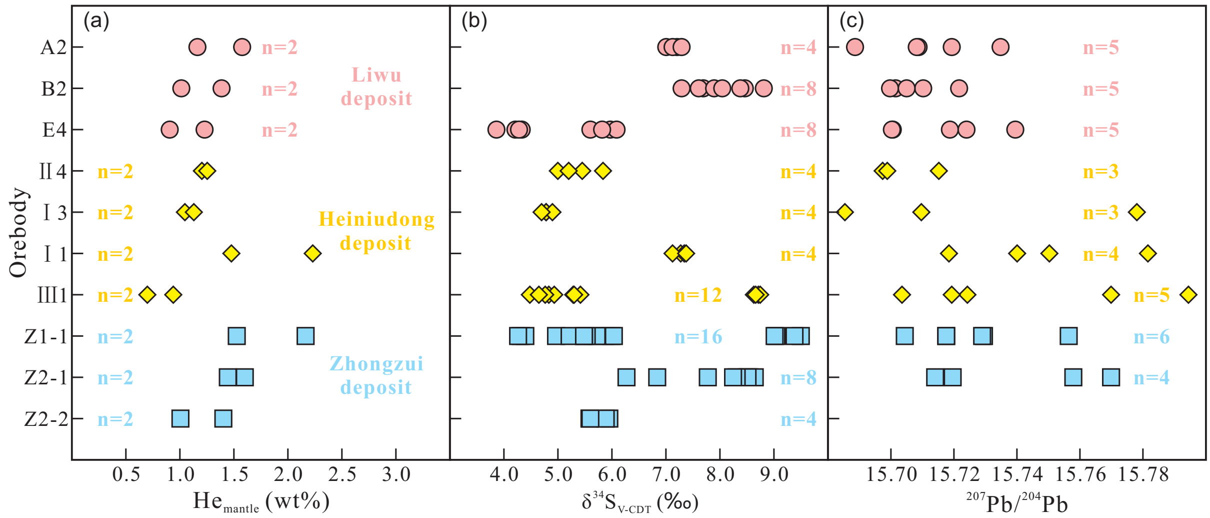

Figure 11. Comparison of He$_{mantle}$ (a), $\delta^{34}S_{V-CDT}$ (b) and $^{207}Pb/^{204}Pb$ (c) values for different orebodies of stratiform Cu deposits in the Jianglang Dome.

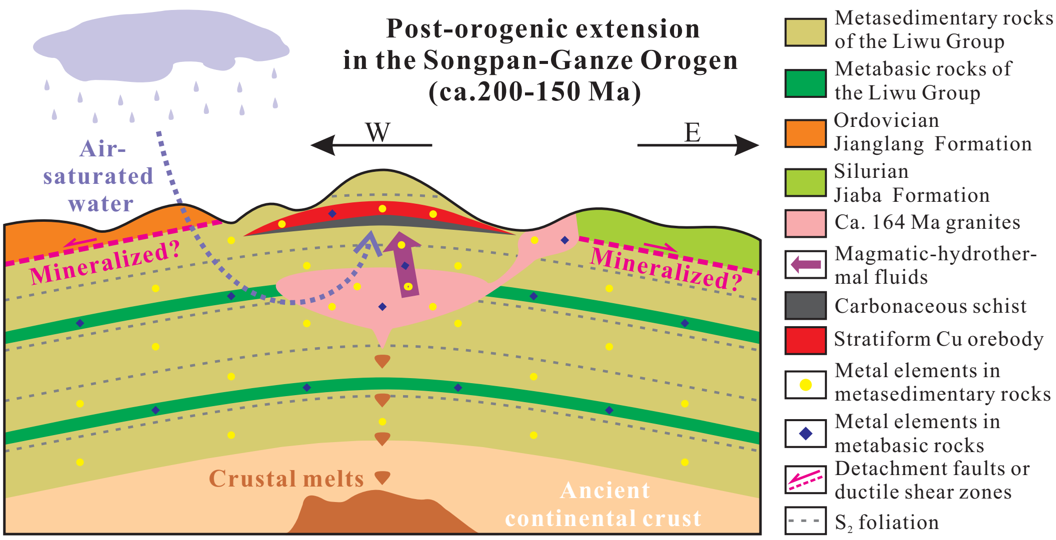

Figure 12. Conceptual model (not to scale) showing an epigenetic and crustal origin of stratiform Cu deposits in the Jianglang Dome.

the Jianglang Dome. This is further supported by: (1) low residual gravity anomalies in the core of the Jianglang Dome (Figure 1e), implying a large deep-seated granitic batholith (e.g. Mangkhemthong *et al.* 2020); (2) magmatic-hydrothermal affinities evidenced by chalcopyrite in situ sulphur isotope data ($\delta^{34}S_{V-CDT}$ = 3.87–9.50‰, Figure 9c), chalcopyrite and granite Pb isotope compositions (Figure 10), as well as boron isotope data of ore-associated tourmalines ($\delta^{11}B$ = −15.47 ± 0.83‰ to −5.91 ± 0.67‰, Zhou *et al.* 2017); and (3) ore-forming fluids related to magmatism, with temperatures of 142–375 °C and salinities of 5.26–21.19 wt.% NaCl equiv., according to recent fluid inclusion data (Yuan *et al.* 2023). In contrast, the Triassic orogenic event (Roger *et al.* 2010; Xu *et al.* 2020) and peak metamorphism at ca. 204–190 Ma (Huang *et al.* 2003a, 2003b) in the Songpan-Ganze Orogen, were not responsible for the ca. 163 Ma epigenetic magmatic-hydrothermal mineralization event in the Jianglang Dome. However, the Triassic synorogenic fluids might yield fine-grained garnets in the Liwu Group, which were elongated and deformed along the S_2 foliation (Figure 6a) due to the Jurassic post-orogenic extension in the Songpan-Ganze Orogen (Roger *et al.* 2010).

In the vertical direction, multiple en-echelon-shaped Cu orebodies are distributed in the Liwu, Heiniudong and Zhongzui stratiform deposits (Figures 5 and 6). Perfectly, these Cu orebodies show similar He-Ar-S-Pb isotope compositions (Figure 11), indicating their source homogeneity and a unified mineralization system. This is contrasting to classic SSC deposits, which commonly show heterogeneous S-Pb-Sr-Nd isotopic features (e.g. El Desouky *et al.* 2010; Panneerselvam *et al.* 2012; Van Wilderode *et al.* 2015). Indeed, almost all sulphide mineralization within the Liwu Group occurs along the S_2 foliation (Figure 4c, d and f). However, the orebodies are delineated by a cut-off Cu grade of 0.4% in the Jianglang Dome, leading to minor lenticular geometries and apparent oblique cross-cutting in some locations (Figure 5). According to field geological mapping, hydrothermal alteration halos are stably and annularly distributed in the Jianglang Dome, and all the discovered stratiform Cu deposits occur near their surface extension (Figure 1c and d). This is suggestive of significant mineral exploration potential in blank areas of this dome. Emphatically, homologous domes in the eastern Songpan-Ganze Orogen, where fertile basement rocks (such as the Late Neoproterozoic Liwu Group) and magmatic-hydrothermal systems are present, likely have Cu mineralization potential, e.g. the adjacent Taka Dome to the north of the Jianglang Dome (Figure. 1c and d).

Taken together, all the data, our preferred genetic scenario for the investigated stratiform Cu-sulphide deposits is established as follows. In the Neoproterozoic of ca. 545 Ma, a volcano-sedimentary sequence (the Liwu Group protoliths) with primary metal enrichment was deposited in a back-arc basin, and thus provided a primitive metal reservoir (Dai *et al.* 2025a). During the post-orogenic extensional setting at ca. 200–150 Ma in the Songpan-Ganze Orogen (Roger *et al.* 2004, 2010), the decompression melting of ancient continental crust formed crustal melts and a large deep-seated granitic batholith with low residual gravity anomalies (Fig. 1e). At ca. 164 Ma, the magma intruded across the fertile Liwu Group, absorbed metallic elements and formed sulphide-bearing granite in some locations (Figure 3b). Due to the low proportion of sandwiched metabasic rocks in the Liwu Group (total <5 vol%), the crust-derived magmatic-hydrothermal fluids contained only 0.69–2.20 wt.% mantle components. These cupriferous crustal fluids mixed with minor air-saturated water, leached fertile host rocks and extracted metals (Virtanen *et al.* 2021). They then transported across the black carbonaceous schists (Figure. 3e and f), which acted as a reduction front for cupriferous hydrothermal fluids (Hitzman *et al.* 2010; Borg *et al.* 2012; Brown, 2014), and finally triggered stable copper sulphide precipitation (Figure 12).

6. Conclusions

In this study, an integration of sulphide Re-Os and He-Ar-S-Pb isotope data offers important insights into mineralization age and origin of stratiform Cu deposits in the Jianglang Dome. The conclusions can be summarized as:

(1) Chalcopyrite Re-Os isotopic dating defines an isochron age of 162.7 Ma. This is coeval with ca. 164 Ma granites in this region and shows no overlaps with ca. 204–190 Ma peak metamorphism in the Songpan-Ganze Orogen. Combined with geophysical, S-Pb-B isotope and fluid inclusion studies, our age data confirm an epigenetic magmatic-hydrothermal mineralization, involving no synorogenic metamorphic fluids.

(2) Sulphide He-Ar isotope systematics support a dominantly crustal origin with minor air-saturated water for the ore-forming fluids. The calculated He_{mantle} values of 0.69–2.20 wt.% match the low proportion of sandwiched metabasic rocks in the fertile Liwu Group (total <5 vol%). Chalcopyrite in situ S isotope data, together with chalcopyrite Pb isotope results, suggest a genetic link with the ca. 164 Ma granites.

(3) According to He-Ar-S-Pb isotope compositions, all the copper orebodies within the Liwu Group show source homogeneity and a unified mineralization system. This indicates mineral exploration potentials in blank areas of the Jianglang Dome, as well as analogous domes with fertile basement rocks and magmatic-hydrothermal systems in the eastern Songpan-Ganze Orogen.

Supplementary material. The supplementary material for this article can be found at https://doi.org/10.1017/S0016756826100648

Acknowledgements. We thank Fei Su, Qiuyun Yuan, Hongfang Chen and Chao Li for analytical assistances. Special thanks are due to Gaolin Tang and Xianze Zhang for their help during the fieldwork. This research was financially supported by the National Natural Science Foundation of China (42572078, 41902068) and China Geological Survey Project (DD20230338, DD20242494). We are grateful to two anonymous reviewers for their constructive comments and important corrections, as well as efficient editorial handling by Dr. Tim Johnson.

Competing interests. The authors declared that they have no conflicts of interest in this work. We declare that we do not have any commercial or associative interest that represents a conflict of interest in connection with the work submitted.

References.

Audétat A and Edmonds M (2020) Magmatic-hydrothermal fluids. *Elements* **16**, 401–06.

Ballentine CJ, Burgess R and Marty B (2002) Tracing fluid origin, transport and interaction in the crust. *Reviews in Mineralogy and Geochemistry* **47**, 539–614.

Bernau R, Roberts S, Richards M, Nisbet B, Boyce A and Nowecki J (2013) The geology and geochemistry of the Lumwana Cu (± Co ± U) deposits, NW Zambia. *Mineralium Deposita* **48**, 137–53.

Borg G, Piestrzynski A, Bachmann GH, Püttmann W, Walther S and Fiedler M (2012) An overview of the European Kupferschiefer deposits. *Society of Economic Geologists, Special Publication* **16**, 455–86.

Brown AC (2014) Low-temperature sediment-hosted copper deposits. In *Treatise on Geochemistry* (second edition, eds HD Holland and KK Turekian), pp. 251–71. Amsterdam: Elsevier.

Cao MJ, Qin KQ, Li GM, Evans NJ, He HY and Jin LY (2015) A mixture of mantle and crustal derived He–Ar–C–S ore-forming fluids at the Baogutu reduced porphyry Cu deposit, western Junggar. *Journal of Asian Earth Sciences* **98**, 188–97.

Dai YP, Zhang HH, Zhu YD, Shen ZW, Li TZ and Ma D (2016) Review on Jianglang dome and Liwu-type copper deposit in the western margin of Yangtze block. *Journal of Earth Sciences and Environment* **38**, 66–78 (in Chinese with English abstract).

Dai YP, Zhu YD, Li TZ, Zhang HH, Tang GL and Shen ZW (2017) A crustal source for ca. 165 Ma post-collisional granites related to mineralization in the Jianglang dome of the Songpan-Ganzi Orogen, eastern Tiebtan Plateau. *Chemie der Erde-Geochemistry* **77**, 573–86.

Dai YP, Zhu YD, Liang SX and Zhou Q (2025a) Late Neoproterozoic and fertile metavolcano-sedimentary sequence facilitated epigenetic Cu mineralization in the Jianglang Dome, southeastern Songpan-Ganze Orogen. *Lithos* **500–501**, 107996.

Dai YP, Zhu YD, Liang SX, Li TZ and Zhou Q (2025b) Primary Enrichment and Epigenetic Magmatic-Hydrothermal Reactivation Caused a New Type of Stratiform Cu-Co Deposits in the Jianglang Dome, Eastern Tibetan Plateau. *Bulletin of the Geological Society of America* **137**, 3527–48.

Davey J, Roberts S and Wilkinson JJ (2021) Copper-and cobalt-rich, ultra-potassic bittern brines responsible for the formation of the Nkana-Mindola deposits, Zambian Copperbelt. *Geology* **49**, 341–45.

Dewaele S, Muchez P, Vets J, Fernandez-Alonzo M and Tack L (2006) Multiphase origin of the Cu-Co ore deposits in the western part of the Lufilian fold-and-thrust belt, Katanga (Democratic Republic of Congo). *Journal of African Earth Sciences* **46**, 455–69.

Du AD, Wu SQ, Sun DZ, Wang SX, Qu WJ, Markey R, Stein H, Morgan J and Malinovskiy D (2004) Preparation and certification of Re–Os dating reference materials: Molybdenites HLP and JDC. *Geostandards and Geoanalytical Research* **28**, 41–52.

Du AD, Qu WJ, Wang DH and Li C (2012) Application of the Re–Os dating in economic geology. Geological Publishing House, Beijing, pp. 1–182 (in Chinese).

El Desouky HA, Muchez P and Cailteux J (2009) Two Cu-Co sulfide phases and contrasting fluid systems in the Katanga Copperbelt, Democratic Republic of Congo. *Ore Geology Reviews* **36**, 315–32.

El Desouky HA, Muchez P, Boyce AJ, Schneider J, Cailteux JLH, Dewaele S and von Quadt A (2010) Genesis of sediment-hosted stratiform copper-cobalt mineralization at Luiswishi and Kamoto, Katanga Copperbelt (Democratic Republic of Congo). *Mineralium Deposita* **45**, 735–63.

Fu JL, Hu ZC, Zhang W, Yang L, Liu YS, Li M, Zong KQ, Gao S and Hu SH (2016) In situ, sulfur isotopes (δ^{34}S and δ^{33}S) analyses in sulfides and elemental sulfur using high sensitivity cones combined with the addition of nitrogen by Laser Ablation MC-ICP-MS. *Analytica Chimica Acta* **911**, 14–26.

Gao JG, Xu ZQ, Li GW, Ding F, Das S, Lian DY, Zheng BH, Yan HY, Pan M, Jiang XF and Lu YX (2023) Sources and petrogenesis of Late Triassic granitoids in the Yajiang gneiss dome group (eastern Songpan-Ganze orogenic belt) with tectonic implications. *Ore Geology Reviews* **161**, 105623.

Gautheron C and Moreira M (2002) Helium signature of the subcontinental lithospheric mantle. *Earth and Planetary Science Letters* **199**, 39–47.

Gongalsky B, Velivetskaya T and Taskaev V (2024) Mineral and S-isotope compositions of Cu-sulfide deposits in southern Siberia (Kodar-Udokan region), Russia. *Minerals* **14**, 228.

Goodwin NRJ, Burgess R, Craw D, Teagle DAH and Ballentine CJ (2017) Noble gases fingerprint a metasedimentary fluid source in the Macraes orogenic gold deposit, New Zealand. *Mineralium Deposita* **52**, 197–209.

Guo RQ, Han SJ, Chen YC, Dang HL, Wang JH, Yang YC, Hu SH and Yuan YR (2024) Deciphering ore-forming fluid evolution processes of the Yuerya gold deposit, eastern Hebei, China: Insights from pyrite texture, trace element and sulfur isotope compositions. *Ore Geology Reviews* **171**, 106178.

Hayes TS, Cox DP, Piatak NM and Seal RR II (2015) Sediment-hosted stratabound copper deposit model. *U.S. Geological Survey Scientific Investigations Report* 2010–5070–M, 1–147.

He HY, Zhu RX and Saxton J (2011) Noble gas isotopes in corundum and peridotite xenoliths from the eastern North China Craton: Implication for comprehensive refertilization of lithospheric mantle. *Physics of the Earth and Planetary Interiors* **189**, 185–91.

Hitzman MW, Selley D and Bull S (2010) Formation of sedimentary rock-hosted stratiform copper deposits through Earth history. *Economic Geology* **105**, 627–39.

Höhn S, Frimmel HE, Debaille V, Pašava J, Kuulmann L and Debouge W (2017) The case for metamorphic base metal mineralization: Pyrite chemical, Cu and S isotope data from the Cu-Zn deposit at Kupferberg in Bavaria, Germany. *Mineralium Deposita* **52**, 1145–56.

Horn S, Gunn AG, Petavratzi E, Shaw RA, Eilu P, Törmänen T, Bjerkgård T, Sandstad JS, Jonsson E, Kountourelis S and Wall F (2021) Cobalt resources in Europe and the potential for new discoveries. *Ore Geology Reviews* **130**, 103915.

Hu RZ, Burnard PG, Bi XW, Zhou MF, Peng JT, Su WC and Zhao JH (2009) Mantle-derived gaseous components in ore-forming fluids of the Xiangshan uranium deposit, Jiangxi province, China: Evidence from He, Ar and C isotopes. *Chemical Geology* **266**, 86–95.

Huang MH, Buick IS and Hou LW (2003a) Tectonometamorphic evolution of the eastern Tibet Plateau: Evidence from the central east Songpan-Garze orogenic belt, western China. *Journal of Petrology* **44**, 225–78.

Huang M, Maas R, Buick IS and Williams IS (2003b) Crustal response to continental collisions between the Tibet, Indian, South China and North China blocks: Geochronological constraints from the Songpan-Garze orogenic belt, western China. *Journal of Metamorphic Geology* **21**, 223–40.

Kendrick MA, Burgess R, Pattrick RAD and Turner G (2001) Fluid inclusion noble gas and halogen evidence on the origin of Cu-porphyry mineralising fluids. *Geochimica et Cosmochimica Acta* **65**, 2651–68.

Li TZ, Zhou Q, Zhang HH, Dai YP, Ma GT, Ma D and Shen ZW (2016) Ore geology and molybdenite Re–Os dating of the Wulaxi tungsten deposit in western Sichuan. *Geological Journal of China Universities* **22**, 423–30 (in Chinese with English abstract).

Liu QP, Mambwe P, Littke R and Muchez P (2024) Diagenesis and mineralization in the Central African Copperbelt, implications from the reflectance of pyrobitumen and Kübler (illite crystallinity) index. *International Journal of Coal Geology* **289**, 104534.

Mamyrin BA and Tolstikhin IN (1984) *Helium Isotopes in Nature.* Amsterdam: Elsevier, pp. 1–273.

Mambwe P, Delvaux D, Dewaele S, Kipata L and Muchez P (2024) Fluid flow in the Katanga Supergroup: From Lufilian brittle tectonic stages to the post-Lufilian period (Democratic Republic of Congo). *Journal of African Earth Sciences* **220**, 105414.

Mangkhemthong N, Morley CK, Kanthiya S and Chaisri S (2020) Geological model and development of the Cenozoic Wiang Pa Pao Basin, Chiang Rai Province, Northern Thailand, based on gravity data modelling and surface structural interpretation. *Tectonophysics* **786**, 228454.

Muchez P, Brems D, Clara E, De Cleyn A, Lammens L, Boyce A, De Muynck D, Mukumba W, Sikazwe O (2010) Evolution of Cu-Co mineralizing fluids at Nkana Mine, Central African Copperbelt, Zambia. *Journal of African Earth Sciences* **58**, 457–74.

Muchez P, André-Mayer AS, El Desouky HA and Reisberg L (2015) Diagenetic origin of the stratiform Cu-Co deposit at Kamoto in the Central African Copperbelt. *Mineralium Deposita* **50**, 437–47.

Mudd GM and Jowitt SM (2018) Growing global copper resources, reserves and production: Discovery is not the only control on supply. *Economic Geology* **113**, 1235–67.

Panneerselvam K, Macfarlane AW and Salters VJM (2012) Reconnaissance lead isotope characteristics of the Blackbird deposit: Implications for the age and origin of cobalt-copper mineralization in the Idaho cobalt belt, United States. *Economic Geology* **107**, 1177–88.

Perelló J, Clifford JA, Creaser RA and Valencia VA (2015) An example of synorogenic sediment-hosted copper mineralization: Geologic and geochronologic evidence from the paleoproterozoic nussir deposit, Finnmark, Arctic Norway. *Economic Geology* **110**, 677–89.

Perelló J, Sillitoe RH, Yakubchuk AS, Valencia VA and Cornejo P (2017) Age and tectonic setting of the Udokan sediment-hosted copper-silver deposit, Transbaikalia, Russia. *Ore Geology Reviews* **86**, 856–66.

Peucker-Ehrenbrink B and Jahn B (2001) Rhenium-osmium isotope systematics and platinum group element concentrations: Loess and the upper continental crust. *Geochemistry Geophysics Geosystems* **2**, 2001GC000172.

Qiu ZJ, Fan HR, Liu X, Yang KF, Hu FF, Xu WG and Wen BJ (2016) Mineralogy, chalcopyrite Re-Os geochronology and sulfur isotope of the Hujiayu Cu deposit in the Zhongtiao Mountains, North China Craton: Implications for a Paleoproterozoic metamorphogenic copper mineralization. *Ore Geology Reviews* **78**, 252–67.

Qiu ZJ, Fan HR, Liu X, Yang KF, Hu FF and Cai YC (2017) Metamorphic P-T-t evolution of Paleoproterozoic schist-hosted Cu deposits in the Zhongtiao Mountains, North China Craton: Retrograde ore formation during sluggish exhumation. *Precambrian Research* **300**, 59–77.

Qiu ZJ, Fan HR, Goldfarb R, Tomkins AG, Yang KF, Li XC, Xie LW and Liu X (2021) Cobalt concentration in a sulfidic sea and mobilization during orogenesis: Implications for targeting epigenetic sediment-hosted Cu-Co deposits. *Geochimica et Cosmochimica Acta* **305**, 1–18.

Roger F, Malavieille J, Leloup PH, Calassou S and Xu Z (2004) Timing of granite emplacement and cooling in the Songpan-Garzê fold belt (eastern Tibetan plateau) with tectonic implications. *Journal of Asian Earth Sciences* **22**, 465–81.

Roger F, Jolivet M and Malavieille J (2010) The tectonic evolution of the Songpan-Garzê (North Tibet) and adjacent areas from Proterozoic to Present: A synthesis. *Journal of Asian Earth Sciences* **39**, 254–69.

Sasaki A and Ishihara S (1979) Sulfur isotopic composition of the magnetite-series and ilmenite-series granitoids in Japan. *Contributions to Mineralogy and Petrology* **68**, 107–15.

Schmandt D, Broughton D, Hitzman MW, Plink-Bjorklund P, Edwards D and Humphrey J (2013) The Kamoa copper deposit, democratic republic of Congo: Stratigraphy, diagenetic and hydrothermal alteration, and mineralization. *Economic Geology* **108**, 1301–24.

Seal RR (2006) Sulfur isotope geochemistry of sulfide minerals. *Reviews in Mineralogy and Geochemistry* **61**, 633–77.

Selley D, Broughton D, Scott R, Hitzman M, Bull S, Large R, McGoldrick P, Croaker M, Pollington N and Barra F (2005) A new look at the geology of the Zambian copperbelt. In *Economic Geology 100th Anniversary Volume* (eds JW Hedenquist, JFH Thompson, RJ Goldfarb and JP Richards), pp. 965–1000. Littleton: Society of Economic Geologists.

Shirey SB and Walker RJ (1995) Carius tube digestion for low-blank rhenium-osmium analysis. *Analytical Chemistry* **67**, 2136–41.

Sillitoe RH, Perelló J, Creaser RA, Wilton J, Wilson AJ and Dawborn T (2017) Age of the Zambian Copperbelt. *Mineralium Deposita* **52**, 1245–68.

Steiger RH and Jäger E (1977) Subcommission on geochronology: Convention on the use of decay constants in geo-and cosmochronology. *Earth and Planetary Science Letters* **36**, 359–62.

Stuart FM, Burnard PG, Taylor RP and Turner G (1995) Resolving mantle and crustal contribution to ancient hydrothermal fluids: He–Ar isotopes in fluid inclusions from Dae Hwa W–Mo mineralization, South Korea. *Geochimica et Cosmochimica Acta* **59**, 4663–73.

Taylor R and McLennan SM (1985) *The Continental Crust: Its Composition and Evolution*. Oxford: Blackwell, pp. 1–328.

Van Wilderode J, Debruyne D, Torremans K, Elburg MA, Vanhaecke F and Muchez P (2015) Metal sources for the Nkana and Konkola stratiform Cu–Co deposits (Zambian Copperbelt): Insights from Sr and Nd isotope ratios. *Ore Geology Reviews* **67**, 127–38.

Vermeesch P (2018) IsoplotR: A free and open toolbox for geochronology. *Geoscience Frontiers* **9**, 1479–93.

Virtanen VJ, Heinonen JS, Molnár F, Schmidt MW, Marxer F, Skyttä P, Kueter N and Moslova K (2021) Fluids as primary carriers of sulphur and copper in magmatic assimilation. *Nature Communications* **12**, 1–12.

Weis D, Kieffer B, Maerschalk C, Barling J, De Jong J, Williams GA, Hanano D, Pretorius W, Mattielli N, Scoates JS, Goolaerts A, Friedman RM and Mahoney JB (2006) High-precision isotopic characterization of USGS reference materials by TIMS and MC-ICP-MS. *Geochemistry Geophysics Geosystems* **7**, 1–30.

Weislogel AL, Graham SA, Chang EZ, Wooden JL and Gehrels GE (2010) Detrital zircon provenance from three turbidite depocenters of the Middle–Upper Triassic Songpan-Ganzi complex, central China: Record of collisional tectonics, erosional exhumation, and sediment production. *Bulletin of the Geological Society of America* **122**, 2041–62.

Xu ZQ, Fu XF, Wang RC, Li GW, Zheng YL, Zhao ZB and Lian DY (2020) Generation of lithium-bearing pegmatite deposits within the Songpan-Ganze orogenic belt, East Tibet. *Lithos* **354–355**, 1–11.

Yan DP, Song HL, Fu ZR and Tian JY (1997) *Metamorphic Core Complexes in the Western Margin of the Yangtze Platform*. Beijing: Geological Publisher House, pp. 1–194 (in Chinese with English abstract).

Yan DP, Zhou MF, Song HL and Fu ZR (2003) Structural style and tectonic significance of the Jianglang dome in the eastern margin of the Tibetan Plateau, China. *Journal of Structural Geology* **25**, 765–79.

Yuan HY, Zhou Q, Song YB, Zhang W, Zhang HH, Li TZ, Yin T, Wang CN and Tang GL (2023) Mineralization of the Liwu large-scale stratiform copper deposits in Sichuan Province, China: Constraints from fluid inclusions. *China Geology* **6**, 252–68.

Zartman R and Doe B (1981) Plumbotectonics the model. *Tectonophysics* **75**, 135–62.

Zhang HF, Parrish P, Zhang L, Xu WC, Yuan HL, Gao S and Crowley QG (2007) A-type granite and adakitic magmatism association in Songpan-Garze fold belt, eastern Tibetan Plateau: Implication for lithospheric delamination. *Lithos* **97**, 323–35.

Zhang HH, Feng XL, Tang GL, Zhou Q, Li TZ, Zhu XP, Wu ZB and Xia XB (2013) Structure types and mineralization in the Zhongzui copper deposit, Jiulong County, Sichuan Province. *Geological Journal of China Universities* **19**, 95–108 (in Chinese with English abstract).

Zhao Y, Li NB, Jiang YH, Niu HC and Yang WB (2018) Multi-stage Cu remobilization of the Huping metamorphic-hydrothermal deposit in the southern North China Craton. *Ore Geology Reviews* **101**, 870–84.

Zhou Q, Li WC, Zhang HH, Li TZ, Yuan HY, Feng XL, Li C, Liao ZW and Wang SW (2017) Post-magmatic hydrothermal origin of late Jurassic Liwu copper polymetallic deposits, western China: Direct chalcopyrite Re–Os dating and Pb–B isotopic constraints. *Ore Geology Reviews* **89**, 526–43.

Zhu BQ (1998) *The Isotope System and its Application in Geology*. Beijing: Science Press, pp. 1–330 (in Chinese).

Zhu ZM and Sun YL (2013) Direct Re–Os dating of chalcopyrite from the Lala IOCG deposit in the Kangdian copper belt, China. *Economic Geology* **108**, 871–82.

Zhu YD, Dai YP, Wang LL, Xiu D and Chen C (2020) Geochemical and isotopic compositions of Late Permian metavolcano-sedimentary sequence in the southern Songpan-Ganzi Orogen, eastern Tibetan Plateau. *Geological Magazine* **157**, 2004–20.